A differential requirement for ciliary transition zone proteins in human and mouse neural progenitor fate specification

Antonia Wiegering[1,*], Isabelle Anselme[1], Ludovica Brunetti[1], Laura Metayer-Derout[1], Damelys Calderon[2], Sophie Thomas[2], Stéphane Nedelec[3], Alexis Eschstruth[1], Valentina Serpieri[4], Martin Catala[1], Christophe Antoniewski[5], Sylvie Schneider-Maunoury[1,*#], Aline Stedman[1,*#]

[1] Sorbonne Université, Institute of Biology Paris-Seine, Developmental Biology Laboratory, CNRS UMR 7622, Inserm U1156, Paris, France.

[2] INSERM UMR 1163, Institut Imagine, Université Paris Cité, Paris, France.

[3] Sorbonne Université, Institut du Fer à Moulin, Inserm UMR-S 1270, Paris, France.

[4] Department of Molecular Medicine, University of Pavia, Pavia, Italy.

[5]ARTbio Bioinformatics Analysis Facility, Sorbonne Université, Institut de Biologie Paris Seine, CNRS FR 3631, Paris, France.

*co-corresponding authors

#co-last authors

Abstract

Studying developmental processes in the context of the human central nervous system is essential to understand neurodevelopmental diseases. In this paper we perform a comparative functional study of the ciliopathy gene *RPGRIP1L* in human and mouse spinal development using *in vitro* 3D differentiation of pluripotent stem cells. *RPGRIP1L*, a causal gene of severe neurodevelopmental ciliopathies such as Joubert and Meckel syndromes, encodes a scaffolding protein of the ciliary transition zone involved in ciliary gating. Previous work has identified a major role for *Rpgrip1l* in mouse brain and spinal cord development, via controlling the Sonic Hedgehog (SHH)/GLI pathway. We show that spinal organoids derived from *Rpgrip1l* mutant mouse embryonic stem cells faithfully recapitulate the loss of motoneurons and the strong reduction of SHH signaling observed in the mutant mice. In contrast, human induced pluripotent stem cells mutant for *RPGRIP1L* produce motoneurons and activate the SHH pathway at levels similar to wild types, a property shared by human iPSCs mutant for another ciliopathy gene *TMEM67*. Moreover, we show that, in human *RPGRIP1L* mutant organoids, motoneurons acquire a more anterior identity, expressing *HOX* genes and proteins normally present in the hindbrain while motoneurons from wild type organoids strictly display spinal identity. By performing a temporal transcriptome analysis throughout the differentiation process, we find that the anteroposterior specification defect arises in early axial progenitors and correlates with the loss of cilia in these cells. Thus, this study uncovers distinct functions in humans and mice for ciliopathy proteins and a novel role for RPGRIP1L in human spinal anteroposterior patterning. These findings have important implications for understanding the role of cilia in human spinal cord development and the pathogenic mechanisms of neurodevelopmental ciliopathies.

Introduction

Primary cilia are highly conserved signaling organelles that protrude from the surface of most vertebrate cells. Constructed from a microtubule scaffold, the ciliary axoneme is anchored in the plasma membrane via the basal body, a modified mother centriole. A specific structure above the basal body, the ciliary transition zone (TZ), regulates the entry and exit of proteins, thereby acting as a "ciliary gate" that regulates the composition of cilia and creates an independent cell compartment. By modulating several signaling pathways such as SHH, WNT and PDGFR, cilia play essential roles in embryonic development and adult tissue homeostasis. Consequently, defects in primary cilia can lead to a large group of genetically and phenotypically heterogeneous syndromes called ciliopathies [1, 2].

Interestingly, although ubiquitously present, mutations in ciliary genes lead to very diverse pathologies that can affect organs like the retina, kidneys, lung, heart and the central nervous system (CNS) whereby the symptoms caused by ciliary mutations greatly vary based on the mutated protein but also between patients even in the same family. Nonetheless, some correlations can be drawn between groups of mutated genes based on the localization and possibly the function of their protein product, and the ciliopathy syndrome to which mutations in these genes are associated. Although this is not completely deterministic, mutations in genes encoding ciliary TZ proteins often lead to neurodevelopmental ciliopathies such as Joubert Syndrome (JS) and the embryonic lethal Meckel Gruber syndrome (MKS) [1, 3]. Most of the current knowledge about neurodevelopmental defects in ciliopathy patients and their underlying mechanisms was gained by *in vivo* studies on animal models and *in vitro* analyses. Using these approaches, it was demonstrated that primary cilia are present throughout the neuronal lineage, from neural stem cells to progenitor cells, mature neurons and glia, where they play an essential role in CNS formation by modulating signaling pathways and cell cycle progression [4-10]. We and others have demonstrated that the JS causal gene *RPGRIP1L* encodes a large scaffolding protein acting as a keystone of TZ construction [11-26]. In addition, it regulates proteasomal activity at the ciliary base and autophagy in murine cells [27, 28] and is involved in planar cell polarity in zebrafish and mice [29]. Furthermore, an essential function for Rpgrip1l in SHH signaling was demonstrated in mouse embryonic tissues and cultured cells [11, 15, 16, 30]. However, our understanding of the role of RPGRIP1L and other ciliary proteins in human neural fate is still very partial and has been hampered due to the paucity of human models, limiting our ability to understand the role of cilia in human development, and the origin of neural developmental defects in ciliopathies. Moreover, evidence suggests that primary cilia function could be only partially overlapping between human and animal models, partly due to specificities in human CNS development. For example, while *Rpgrip1l* mutant mouse embryos, like other ciliary mutants, display a severe disorganization of the ventral diencephalic and hypothalamic regions and of the ventral spinal cord, no such phenotype was described in ciliopathy patients [6, 7, 31-33].

In this study, we took advantage of pluripotent stem cell-based organoid approaches to study the role of the TZ proteins RPGRIP1L and TMEM67 in human neural progenitor (NP) fate. Since the role for

ciliary proteins in SHH-dependent patterning of the ventral spinal cord has been largely studied, we used wild-type (WT) and Rpgrip1l-deficient mouse embryonic stem cell (mESC)- and human induced pluripotent stem cell (hiPSC)-derived spinal organoids to compare the functions of RPGRIP1L in ciliogenesis and spinal progenitors between these two models. We show that mouse *Rpgrip1l*$^{-/-}$ organoids exhibit altered dorso-ventral patterning in response to SHH, similar to mutant mouse embryos, emphasizing the cell-intrinsic requirement for Rpgrip1l in spinal progenitors for cilia-dependent SHH pathway activation and commitment into ventral neuronal cell types. In contrast, RPGRIP1L-deficient human iPSCs submitted to a similar differentiation protocol are still able to form primary cilia and adopt SHH-dependent ventral spinal fates. Interestingly, this phenotype is not unique to RPGRIP1L deficiency, but is also observed in TMEM67-deficient human ventral organoids. TMEM67 belongs to the MKS/B9 module of the TZ and likewise RPGRIP1L, has been shown to regulate SHH-dependent spinal patterning in mouse models [8, 34-36]. Remarkably, in addition to the species-specific differences of TZ proteins in cilia formation and signaling between mouse and human, we discovered a novel role for the human RPGRIP1L protein in the precise assignment of antero-posterior (rostro-caudal) identities of human spinal progenitors. Indeed, mutant motoneurons (MNs) derived from early neuromesodermal progenitors shift their identity from thoracic to more rostral/hindbrain identities. This is accompanied by a temporary loss of cilia in RPGRIP1L-deficient axial progenitor cells. With this study, we bring a first proof of concept that inter-species differences can be dissected by dynamically comparing mouse and human *ex vivo* organoids and we highlight new human-specific functions for the ciliopathy gene *RPGRIP1L* in antero-posterior patterning of axial progenitors.

Results

Defective SHH-induced motoneuron specification in *Rpgrip1l* KO mouse spinal organoids

In vertebrates, graded SHH signaling along the dorso-ventral (DV) axis of the spinal cord is necessary for the specification of the floorplate (FP) and the four different ventral progenitor domains p3, pMN, p2 and p1 (Figure 1A) [37-44]. The study of mouse ciliary mutant embryos demonstrated that primary cilia are required for SHH transduction and the correct establishment of spinal DV patterning [15, 45-48]. In *Rpgrip1l*$^{-/-}$ (KO) mouse embryos, brain and spinal cord progenitors lack a functional cilium, leading to altered SHH pathway activation and repression [6, 7, 15, 16]. As a consequence, in the spinal cord, the FP and p3 territories are not established, fewer pMNs are specified and the dorsal domains are shifted ventrally [6, 15]. In order to test whether this phenotype can be reproduced *ex vivo*, even under conditions where SHH activation is forced by the addition of a constant dose of SHH agonist (Smoothened AGonist, SAG), we established WT and *Rpgrip1l KO* mESC lines from mouse blastocysts that we differentiated into ventral spinal organoids [49, 50]. Briefly, mESC are differentiated into embryoid bodies (EBs) in N2B27 neuralizing medium for 2 days (d0-d2). EBs are then targeted to an axial spinal fate by combined exposure to the WNT agonist CHIR99021 and retinoic acid (RA), and further ventralized by addition of SAG. This leads to the transient production of neuromesodermal-like (NMPs-like) bi-potent axial progenitors between day 2 and day 3, characterized by their co-expression of the mesodermal marker Brachyury and the neural markers Sox1 and Sox2 [51-55]. By day 4, axial progenitors have committed into the neuronal spinal lineage and adopt different ventral identities. EBs are let to differentiate into ventral spinal organoids until day 7 (Figure 1B). WT and *Rpgrip1l KO* spinal organoids were collected at different time points of differentiation, sectioned and immunostained to assess the identity of the different progenitors obtained. We found that on average, 50% of spinal progenitors from control organoids committed to a pMN fate by day 4 of differentiation, as evidenced by Olig2 staining (Figure 1C, D). pMNs progressively differentiated into post-mitotic MNs until day 6, a stage when only Islet1-positive MNs could be detected (Figure 1C). Control organoids were also composed of progenitors from the more ventral domains p3 and FP, since we could detect the presence of [Nkx6.1+, Olig2-], Nkx2.2+ and FoxA2+ cells (Figure 1D). Moreover, control organoids nicely recapitulated the sequential activation of ventral neural identities observed *in vivo* in the mouse spinal cord, as *Olig2* expression preceded the initiation of *Nkx2.2* and *FoxA2*. Strikingly, *Rpgrip1l*-deficient progenitors failed to commit to ventral spinal identities. Indeed, the number of Olig2+ and Islet1+ cells of the MN lineage was strongly reduced, while Nkx2.2+ (p3) and FoxA2+ (FP) progenitor cells were nearly absent from mutant organoids (Figure 1C-H). Instead, 80% of the progenitors were positive for PAX6, indicating a shift towards more dorsal identities. To gain a deeper understanding of the changes in cell fate occurring in *Rpgrip1l*-deficient organoids, we performed bulk RNAseq on control and mutant organoids from day 2 to day 7, obtained from 3 independent differentiation experiments (Figure S1A). Our transcriptomic analysis confirmed the shift towards dorsal identities in *Rpgrip1l* mutant organoids, and showed that SHH-dependent ventral cell types were replaced by progenitors expressing

markers characteristics of the p0-p2 domains such as *Dbx1* (Figure 1I, K). Consistently, the molecular signature of post-mitotic neurons changed from V3-MNs in the control, to V1-V0 in *Rpgrip1l* KO organoids (Figure 1J, K). The temporal analysis of the pan-neural markers *Sox1* and *Tuj1* expression in the time course of the differentiation (Figure S1B, S1C) showed that the reduction in MNs correlated with a transient decrease in neurogenesis between days 3 and 7 in *Rpgrip1l* KO compared with control organoids. Since MNs are the first neurons to differentiate in the spinal cord, this result is in line with the dorsalization occurring in the mutant organoids. In *Rpgrip1l* mutant mice, the defective patterning of the ventral spinal cord has been attributed to an absence of primary cilia in spinal progenitors, and the consequent defect in SHH pathway activation [6, 15]. Interestingly, the Ensemble Gene Set Enrichment Analysis (EGSEA) performed on differentially expressed genes in day 3 and day 4 organoids showed an enrichment in genes related to spinal patterning (Figure S1D) and SHH signaling (Figure S1E). Consistently, while expression of direct targets of the pathway, *Gli1*, *Patched1* and *Gli2* was upregulated in controls from day 2, upon SAG addition into the EB culture medium, their expression barely increased in the mutants, showing impaired activation of SHH transduction in absence of Rpgrip1l (Figure 2A, B, C). Finally, to test whether this phenotype was correlated with defective ciliogenesis we analyzed the ciliary marker ADP Ribosylation Factor Like GTPase 13b (Arl13b) by immunostaining on organoid sections. We found that similar to what was observed *in vivo*, *Rpgrip1l* deficiency led to a drastic reduction of the ciliary Arl13b amount (Figure 2D, E). This phenotype might reflect a ciliary gating defect, or an absence of ciliary axoneme. To discriminate between these scenarios, we labeled the axonemal protein Ift88 and measured the length of Ift88 staining to evaluate the axonemal length. We found that the axoneme of mutant progenitors was abnormally stunted, with a mean length of 0.2 µm compared to 1 µm in the control (Figure 2D, F), suggesting that only the TZ might be present above the basal body. This ciliary phenotype was correlated with the complete absence of Rpgrip1l at the ciliary TZ in mutant organoids (Figure 2D). Overall, our results demonstrate that, as *in vivo*, Rpgrip1l is required *in vitro* in mouse spinal progenitors for ciliogenesis, SHH pathway activation and the consequent acquisition of spinal ventral identities. These results provide the first proof of concept that spinal organoids differentiated from pluripotent stem cells (PSCs) constitute a good model to study the consequences of ciliary gene deficiencies on neural cell fate.

Human RPGRIP1L-deficient neural progenitors differentiate into MNs in spinal organoids

To tackle the function of primary cilia and the TZ protein RPGRIP1L in human spinal development and SHH transduction, we generated human iPSC clones deficient for RPGRIP1L (*RPGRIP1L*$^{-/-}$) via introduction of *InDel* mutations that lead to premature STOPs in two independent hiPSC lines (Figure S2). An additional clone, carrying a full deletion of RPGRIP1L (Δexon3-exon27), was also obtained (Figure S3A, B). Validated clones from both hiPSC lines (Ph2 and Wtc11; Figures S2, S3A, B) were used for differentiation into ventral spinal organoids following a well-established 3D differentiation

protocol (Figure 3A) [56, 57]. Importantly, for each genotype, Wtc11 and Ph2 hiPSC lines behaved the same in terms of differentiation efficiency, cilia phenotype and gene expression profiles.

Starting the differentiation of ventral spinal organoids from single cell hiPSCs, EBs were formed after one day in a floating culture in neural induction medium (dual SMAD inhibition) containing the GSK-3β antagonist CHIR99021 for moderate WNT activation (Figure 3A). Within four days, WT and RPGRIP1L-deficient cells adopted a caudal NMP-like axial fate. From day 4 onwards, axial progenitors were treated with RA and high concentrations of SAG in order to induce a ventral neural fate (Figure 3A). At day 6 of ventral spinal organoid differentiation, the majority of control and RPGRIP1L-deficient cells expressed SOX2 and PAX6, both markers of early NPs, indicating that control cells as well as RPGRIP1L-deficient cells adopted the neural fate (Figure S4A). From day 6 onwards, SOX2 and PAX6 expression decreased corresponding to the ongoing specification and differentiation process. In response to SAG stimulation, the MN progenitor (pMN) marker OLIG2 started to be expressed between day 4 and day 6 of differentiation with an expression peak reached at day 9 where 75% of the cells within organoids expressed OLIG2 (Figure 3B and Figure S4B). Combined to that, cells expressed the broad ventral marker NKX6.1 at day 9 of differentiation, further evidence of ventral spinal fate specification (Figure S4B).

Surprisingly, no difference in OLIG2 and NKX6.1 pattern was observed between control and RPGRIP1L-deficient organoids (Figure 3B and Figure S4B). In line with this, control and RPGRIP1L-deficient cells started to express *ISLET1* (*ISL1)* and *ISLET2* (*ISL2*), markers for postmitotic MNs, from day 9 onwards (Figure S4C, D, E). A final treatment of organoids with a γ-Secretase Inhibitor (DAPT) was used to inhibit NOTCH signaling and accelerate the neural differentiation into postmitotic MNs from day 9 onwards (Figure 3A). Consequently, *ISL1* and *ISL2* RNA and protein levels were strongly upregulated within WT and RPGRIP1L-deficient organoids between day 11 and day 14 (Figure 3B, Figure S3D and Figure S4C, D, E). Taken together, these results show that RPGRIP1L-deficient hiPSCs are able to correctly process differentiation from stem cells to NPs and further from pMNs to postmitotic MNs. Nevertheless, our data reveal 15 % less ISL1/2+ MNs at the end of differentiation in RPGRIP1L-deficient hiPSC-derived spinal organoids compared to controls (Figure 3B).

By analyzing the expression of various transcription factors that are distinctly expressed in specific DV regions of the developing spinal cord using bulk RNAseq data, we tested whether, despite the normal pMN production, human iPSC-derived organoids deficient for RPGRIP1L exhibited a shift in DV patterning towards the dorsal domains, as it was demonstrated for mESC-derived *Rpgrip1l KO* spinal organoids (Figure 1, Figure 2). The unaltered expression of the broad ventral marker *NKX6.1*, the intermediate markers *DBX1* and *DBX2*, and the dorsal spinal markers *PAX3*, *PAX7*, and *ZIC1* (Figure 3C, C') during differentiation, indicated that, contrary to mouse Rpgrip1l-deficient spinal organoids, human RPGRIP1L-deficient spinal organoids did not display a more dorsal progenitor type specification. We noted minor changes among the markers *MSX1* and *OLIG3* at day 2 and day 4 in

RPGRIP1L KO organoids, likely reflecting subtle differences in axial progenitor identities, before dorso-ventral neural specification.

To investigate whether the mildly reduced number of MNs in RPGRIP1L-deficient organoids could be caused by a delayed neurogenesis, we analyzed the expression of the global neuronal markers *TUJ1* and *MAP2*. As expected, expression of both markers increased during differentiation with the highest expression of *TUJ1* and *MAP2* between day 11 and day 14 (Figure 3E and Figure S4G) and high protein levels of TUJ1 at day 14 (Figure 3E). Comparing WT and RPGRIP1L-deficient organoids, no significant differences between *MAP2* and *TUJ1* expression on RNA or protein level could be observed. In conclusion, neurogenesis appears unaltered and seems not to be responsible for the slightly reduced number of MNs observed in RPGRIP1L-deficient spinal organoids.

Surprisingly, *NKX2.2* RNA and protein expression was significantly increased at day 11 of MN differentiation in RPGRIP1L-deficient cells (Figure 3C, D). NKX2.2 is expressed in a specific subpopulation of ventral spinal MN progenitors in humans, where it is co-expressed with OLIG2 [58]. By performing co-labeling of OLIG2 and NKX2.2 at day 9 and day 11 of differentiation we could not detect any increase in OLIG2+/NKX2.2+ cells in RPGRIP1L-deficient organoids compared to WT controls (Figure 3D and Figure S4F). Consequently, the increased NKX2.2 amount in RPGRIP1L-deficient spinal organoids is unlikely to be caused by increased numbers of ventral and human-specific MN subtypes. NKX2.2 is also expressed in the most ventral NPs (p3) and neuronal subtype (V3) within the neural tube (Figure 1A). Here, expression of NKX2.2 plays a primary role in ventral neuronal patterning and requires high SHH signaling [59] raising the question about the status of SHH signaling in human RPGRIP1L-deficient spinal organoids.

RPGRIP1L deficient spinal neural progenitor possess cilia and transduce SHH signaling

To determine SHH pathway activity in WT and RPGRIP1L-deficient spinal organoids, we analyzed the expression of SHH target genes *GLI1* and *PTCH1* along the entire spinal differentiation protocol using bulk RNAseq data. In both WT and RPGRIP1L-deficient spinal organoids, an increase in *GLI1* and *PTCH1* expression in response to SAG stimulation was observed between day 4 and day 9 of differentiation, followed by an expected decrease in their expression in agreement with the removal of SAG from the differentiation medium. No significant difference in SHH target gene expression could be observed between WT and RPGRIP1L-deficient cells (Figure 4A). This result is in line with the functional differentiation of RPGRIP1L-deficient hiPSCs into OLIG2+ pMNs and ISL1/2+ postmitotic MNs that highly depends on SHH signaling transduction. In contrast, the earlier described increase in number of NKX2.2+ cells in RPGRIP1L-deficient spinal organoids (Figure 3C-D and Figure S4F) cannot be explained by an increased SHH pathway activity leading to a ventralization effect in RPGRIP1L-deficient spinal organoids.

Based on the results of functional SHH transduction and MN differentiation in human RPGRIP1L-deficient spinal organoids, we expected RPGRIP1L-deficient spinal organoids to possess cilia. We

analyzed cilia formation at day 6 of MN differentiation, a time point where organoids were stimulated with SAG in order to activate SHH signaling and started to adopt the pMN fate. In WT organoids, short primary cilia were detectable on cells lining the outside or the inner lumens of the organoids, thereby pointing into the external environment or the internal cavities (Figure 4B). These cilia were IFT81-positive and displayed a mean length of 1.3 µm (Figure 4C). RPGRIP1L was present at the ciliary transition zone in WT spinal organoids (Figure 4D and Figure S2C, S3C). In RPGRIP1L-deficient organoids, RPGRIP1L was not detectable at the ciliary base (Figure 4D and Figure S2C, S3C). Despite the loss of RPGRIP1L, cilia were present lining apical surfaces (Figure 4B) and displaying an unaltered mean length of 1.3 µm (Figure 4C). However, while WT cilia accumulated the ciliary membrane markers ARL13B, Inositol Polyphosphate-5-Phosphatase E (INPP5E) and Adenylate Cyclase 3 (AC3), reduced amounts of ARL13B and AC3 but not INPP5E were observed in RPGRIP1L-deficient cilia (Figure 4E, F). This indicates a disrupted ciliary gating in human spinal NPs upon RPGRIP1L deficiency. These results are in line with data from *C.elegans*, different mouse tissues and human cell lines, in which a disrupted TZ organization and in consequence an altered ciliary gating has been described under Rpgrip1l deficiency [19, 21, 23, 24, 60]. Since ciliary gating can be involved in SHH signaling function [2, 17, 61] e.g., by regulating ciliary shuttling of pathway components such as SMO (Smoothened) thereby regulating ciliary GPR161 (G Protein-Coupled Receptor 161) amounts [62-64], we tested whether GPR161-trafficking was disrupted in RPGRIP1L mutant spinal organoids. GPR161 was enriched in the ciliary membrane in SHH pathway-inactive WT and RPGRIP1L-deficient cells (Figure S4H). In WT and RPGRIP1L mutant NPs stimulated with SAG, GPR161 did not accumulate within primary cilia and thus did not inhibit SHH pathway activation (Figure S4H). These results are in perfect agreement with the previously described functional SHH pathway activation in WT and RPGRIP1L-deficient spinal organoids and show that ciliary gating defects did not affect SHH signaling transduction in RPGRIP1L-deficient NPs.

To test whether the results obtained with *RPGRIP1L KO* hiPSCs could be extended to other neurodevelopmental ciliopathy genes, we generated TMEM67-deficient hiPSCs via CRISPR/Cas9 from the Ph2 hiPSC line. One control (*TMEM67*$^{+/-}$) and one KO (*TMEM67*$^{-/-}$) clone were used for further analyses (Figure S5A-E). Cilia were present on control and TMEM67-deficient organoids at day 6 of differentiation where they are supposed to transduce SHH signaling (Figure S5C, F). No striking alterations of cilia length or quantity have been observed, nonetheless gating defects might be present indicated by lower ciliary ARL13B intensities (Figure S5C, E). As observed in RPGRIP1L-deficient NPs, gating defects in TMEM67-deficient organoids did not affect SHH transduction in NPs and pMNs as indicated by unaltered SHH target gene expression of *GLI1* and *PTCH1* (Figure S5G, H). Furthermore, control and *TMEM67 KO* organoids started to express *ISL1/2* at day 11 of differentiation (Figure S5I) without significant differences in the ISL1/2+ areas per organoid at day 14 of differentiation (Figure S5J). Thus, human iPSCs mutant for two distinct ciliopathy genes encoding TZ proteins, RPGRIP1L and TMEM67, are able to form cilia, transduce the SHH pathway and differentiate

into MNs, strongly suggesting that human and mouse spinal progenitors react differently to the loss of transition zone proteins.

RPGRIP1L-deficient spinal organoids show antero-posterior patterning defects

Using Principal Component Analysis (PCA) on our dataset, we found that for each time point of the differentiation, WT and RPGRIP1L-deficient organoids clustered together (Figure S6A, B). Furthermore, only minor differences in differential gene expression could be observed by comparing the transcriptome of WT and RPGRIP1L-deficient organoids. Testing for overrepresented gene categories via gene ontology (GOSEQ) analyses did not reveal striking changes in biological processes, molecular functions or cellular components between WT and RPGRIP1L-deficient samples at different time points. Among the few genes that were differentially expressed between WT and RPGRIP1L-deficient organoids, expression of *HOX* genes such as *HOXC6* and *HOXA7* were significantly downregulated in RPGRIP1L-deficient organoids at day 11 and day 14 (Figure S6C, D). In addition, EGSEA on GeneSetDB gene ontology (GO) at day 2 revealed significant downregulation of the biological process *anterior/posterior pattern specification (GO:0009952)* involving downregulation of *HOX* genes such as *HOXA5* and *HOXC6* as well as the *CDX* genes *CDX1*, *CDX2* and *CDX4* (Figure S6E). In addition to the pairwise comparison of WT and RPGRIP1L gene expressions at each selected time point, we performed *differential temporal profiles analyzes* on our data. These analyses revealed additional genes whose expression varied significantly over time (Figure S6F), and that were related to anterior-posterior pattern specification, such as *HOXC8* and *HOXC9* (Figure S6G).

HOX genes are expressed in four clusters along the rostro-caudal axis of bilateral organisms: HOXA, HOXB, HOXC and HOXD. In humans, HOX proteins are encoded by 39 genes whose regionalized expression is realized by their sequential and collinear activation in axial progenitors, which gradually give rise to mesodermal and neuroectodermal structures with rostral and later caudal identity, each expressing a specific HOX code [54, 55, 57, 65, 66]. By analyzing the dynamic expression pattern of the 4 *HOX* gene clusters over time, we identified early differences in the expression of posterior *HOX* genes in RPGRIP1L-deficient organoids compared to controls. In controls, early axial progenitors at day 2 started to express anterior HOX genes such as *HOXA1* followed by activation of later and more posterior HOX genes such as *HOXA7* at day 4 (Figure 5A). At later stages, WT organoids expressed anterior as well as more posterior *HOX* genes of the four different clusters (Figure 5A, B and Figure S7A) such as HOXA genes from *HOXA1* to *HOXA7* (Figure 5A, A') and HOXC genes from *HOXC4* to *HOXC8* (Figure 5B, B'). Consistently, MNs within WT organoids adopted a thoracic antero-posterior identity at day 14, that could be visualized by immunofluorescence labeling of HOXC8, a marker for thoracic MNs (Figure 5C), whereas more anterior HOX genes such as *HOXA5* were not translated at this stage (Figure 5C). During early stages of differentiation, RPGRIP1L-deficient axial progenitors expressed anterior *HOX* genes comparable to the WT situation while expression of more posterior *HOX* genes was already reduced at day 4 (Figure 5A, B). This difference was even more striking at later

stages, where the latest most caudal *HOX* genes expressed in RPGRIP1L-deficient MNs were *HOXA5* instead of *HOXA7* (Figure 5A) and *HOXC4* instead of *HOXC8* (Figure 5B). This result was confirmed at the protein level by immunofluorescence, which showed that RPGRIP1L-deficient MNs failed to express HOXC8, but expressed HOXA5 (Figure 5C, Figure S3E, F). Taken together, the differences in *HOX* gene expression indicate a shift in antero-posterior patterning in RPGRIP1L-deficient organoids in which MNs adopt a more cervical/hindbrain identity than the thoracic spinal identity of WT organoids (Figure 5D) [57, 65, 67].

RPGRIP1L-deficient spinal organoids adopt hindbrain MN identities

By analyzing hindbrain specific pMN and MN markers, we further confirmed the shift in antero-posterior MN identity. *PHOX2B*, a nuclear marker of pMNs and MNs of the hindbrain [68], was expressed in *RPGRIP1L KO* but not WT spinal organoids during differentiation (Figure 5E) and labeled hindbrain MNs in *RPGRIP1L KO* organoids at day 14 of differentiation (Figure 5G). Furthermore, expression of the late hindbrain-specific MN marker *TBX20* [69] was increased in *RPGRIP1L KO* organoids at day 14 (Figure 5F). Based on these results, we hypothesize that the earlier described increase in *NKX2.2* expression (Figure 3C-D) corresponded to the generation of NKX2.2+ hindbrain MNs rather than ventral spinal MNs in RPGRIP1L-deficient organoids [59, 70, 71]. Analyzing earlier markers of hindbrain-specific neural differentiation, the expression of *EGR2/KROX20* [72-75], *FGF3* [75-77], and *NKX2.8*/*NKX2.9* [70, 71] as well as the expression of the early hindbrain pMN marker *PHOX2A* [68, 72, 78] were strikingly increased in RPGRIP1L-deficient organoids at day 4 and day 2, respectively (Figure S7B-F). In contrast, expression of *WNT5A*, which is involved in axis elongation in mammals [79], was decreased in *RPGRIP1L KO* axial progenitors (Figure S7G).

Taken together, our results indicate that the disrupted antero-posterior patterning in RPGRIP1L-deficient organoids leads to the generation of hindbrain MNs instead of spinal MNs.

RPGRIP1L controls axial progenitor fate specification and early ciliogenesis in human spinal organoids

The sequential and collinear expression of *HOX* genes that leads to specification of rostral and later caudal identities is set-up within axial progenitors [53-55, 65, 66, 80-84]. In our human organoid model, cells adopted the axial progenitor fate between day 2 and day 4 of differentiation indicated by coexpression of *CDX2*, *BRACHYURY* and *SOX2* (Figure 6A-C). Interestingly, *CDX2* and *BRACHYURY* expression was equally induced in WT and RPGRIP1L-deficient organoids at day 2 (Figure 6B, C, D). While BRACHYURY expression remained elevated between day 2 to day 4 in WT axial progenitors, it dropped as soon as day 2 in RPGRIP1L-deficient axial progenitors (Figure 6D). Moreover, CDX2 expression was reduced at day 4 in RPGRIP1L-deficient axial progenitors and immunofluorescence appeared patchy, with few clusters of CDX2-negative cells in RPGRIP1L-deficient but not WT organoids (Figure 6E). In addition to *CDX2* and *BRACHYURY*, axial progenitors establish expression

of the spinal cord-specific genes *CDX1* and *CDX4* [85-92]. Both *CDX* genes were expressed in WT spinal cord organoids, with *CDX1* being most highly expressed at day 2 and *CDX4* at day 4 of differentiation (Figure 6F, G). In contrast, induction of *CDX1* expression was strongly reduced and *CDX4* expression strikingly decreased in RPGRIP1L-deficient organoids (Figure 6F, G), further emphasizing the caudal to cranial shift in antero-posterior identity of *RPGRIP1L KO* progenitors.

We analyzed the ciliary status of axial progenitors at day 2 and day 4 of differentiation, and found a strong reduction of cilia number in RPGRIP1L-deficient organoids compared to controls (Figure 6H-J). This contrasts with the presence of cilia in RPGRIP1L-deficient NPs at day 6 (Figure 4B, C), thereby indicating a cell-type specific function of RPGRIP1L in ciliogenesis during spinal differentiation.

We hypothesize that cilia loss in RPGRIP1L-deficient axial progenitors is responsible for the reduced specification or maintenance of axial progenitor fate and the early established antero-posterior patterning defects observed in *RPGRIP1L KO* organoids. In line with this hypothesis, analyses of TMEM67-deficient organoids revealed that cilia were present on control and KO axial progenitors at day 4 of differentiation (Figure S8A, B), and in correlation, no apparent antero-posterior patterning defect could be observed. *HOXC6* and HOXC8 expressions were only slightly altered between control and TMEM67 KO organoids (Figure S8C, D), while *HOXC9* was not expressed (Figure S8E). Importantly, the hindbrain MN marker PHOX2B was not expressed in either control or *TMEM67 KO* organoids (Figure S8F, G). This shows a correlation between the absence of cilia in axial progenitors and the anterior shift in progenitor identity in human spinal organoids. Interestingly, such antero-posterior patterning defect was specific to human spinal progenitors, since no spinal-to-cranial shift was observed in *Rpgrip1l*$^{-/-}$ mouse organoids, as evidenced by the unaltered expression of *Cdx1-2-4*, *Cyp26a1* or *Brachyury* in mutant progenitors compared to controls (Figure S9A-G). Moreover, apart from a slight decrease in HoxPG10 expression, no major alterations were observed in Hox genes expression that might indicate anteroposterior specification defects in the mutants. (Figure S9H-J).

Discussion

TZ proteins are differentially required for ciliogenesis and SHH activation in mouse and human ventral spinal progenitors

Previous analysis of *Rpgrip1l* and *Tmem67* mutant mice demonstrated that deficiency for these TZ proteins led to DV mis-patterning of the neural tube marked by the strong decrease of ventral neuronal subtypes like V3 and MNs [6, 15, 35]. These phenotypes were correlated to the absence of primary cilia and functional SHH signaling, and were also described for *Ift* mutant mice [15, 45-47]. Since these mice are lacking or displaying a reduced FP, a question remained as to whether altered patterning of the neural tube resulted only from a reduced SHH secretion ventrally, or from impairment of SHH signal transduction within ventral spinal progenitors themselves. Here, by exposing control and *Rpgrip1l* mutant spinal organoids to high dose of SHH agonist, we show that primary cilia are intrinsically required within mouse spinal progenitors to transduce SHH. Upon inactive SHH signaling, mutant progenitors switch on intermediate-dorsal identities instead of ventral ones.

Strikingly, we find that contrary to the mouse, human RPGRIP1L and TMEM67 are not required for the establishment of ventral spinal neuronal cell types in organoids. Despite a clear ciliary gating defect, with decreased ARL13B or AC3 ciliary localization, human mutant spinal NPs were still able to grow primary cilia and transduce SHH signaling similarly to controls, adopting MN identities. Ciliogenesis in the absence of Rpgrip1l and Tmem67 has also been observed in other cellular contexts, like in mouse limbs progenitors, MEFs, HEK cells [23, 24, 27, 35] or human fibroblasts derived from *RPGRIP1L* and *TMEM67* mutated JS patients [19, 93]. Whether the difference in ciliary phenotype observed between mouse and human spinal progenitors stems from differences in ciliary composition or stability, and accounts for the difference in SHH activation in these two systems remains to be addressed.

Progenitor-type specificity of cilia defects upon RPGRIP1L deficiency

More generally, in addition to the species-specificity discussed above, our results highlight a context-specific role for ciliary TZ proteins in human neural progenitors. In RPGRIP1L-deficient human organoids, NPs at day 6 display cilia of normal length and a moderately altered ciliary content, while at day 4, axial progenitors display a strong reduction or loss of cilia. Differences in ciliary structure and composition between tissues, already suggested by the high heterogeneity of phenotypes in human ciliopathies, has already been described in other models [23, 94-96]. However, here we show for the first time a change in cilia sensitivity to the loss of a TZ protein along the process of neural progenitor specification in humans, at a key step of cell fate transition.

Whether this change parallels differences in ciliary structure, and which signaling and molecular cascades lead to these changes in cilia stability during the differentiation process are important questions raised by our study. In this regard, recent data show that cell fate can regulate ciliogenesis by different mechanisms such as transcriptional regulation [97], niche condition-specific regulation [98, 99], and several non-canonical signaling pathway activities such as SHH [100] and WNT [101]. It will be an

exciting future task to examine whether these modes of ciliogenesis regulation play a role in diverse spinal NPs and how TZ proteins are involved in it to explain at least in part the regional specificity of defects found in neurodevelopmental ciliopathies.

Establishment of the HOX-code and regulation of antero-posterior patterning

Quite unexpectedly, we found that although they do not display SHH-dependent dorsoventral patterning defects, human RPGRIP1L mutant spinal organoids shift to more anterior identities. Altered anteroposterior patterning could arise from several mechanisms. WNT, RA, Fibroblast Growth Factor (FGF), and more recently NOTCH signaling, have been involved in the determination of axial progenitors and thereby regulation of gradual *HOX* gene expression [57, 85, 102-106]. From our transcriptome data, we could not observe any indication of perturbations in FGF or NOTCH pathways upon RPGRIP1L deficiency. However, we measured a reduced expression of *CDX2*, *CDX1* and *CDX4* as well as a downregulation of the *5-9 HOX* genes, detectable from the very early stages of the differentiation. Analysis of Wnt3a- and Cdx-deficient mouse embryos [86, 107-112] or experimental manipulation of Cdx or BRACHYURY activity [112-116] lead to a working model in which early *BRACHYURY* and subsequent *CDX* expression activates and fine-tunes *HOX* gene expression profiles along the anterior-posterior axis downstream of WNT/β-Catenin signaling in axial progenitors [53, 81, 85, 88, 102, 107, 114-122]. Interestingly, it was demonstrated recently that WNT signaling during early differentiation of hiPSCs into spinal MNs allows progressive, collinear HOX activation and that a switch to RA treatment at any time point during this process stops collinear HOX activation and favors transition into neuroectodermal progenitors with a discrete HOX gene profile [57, 102]. Thus, we hypothesize that the shift in antero-posterior patterning that we describe in RPGRIP1L-deficient human spinal organoids could result from reduced WNT transduction during early stages of axial progenitors differentiation, leading to a reduction in *BRACHYURY*, *CDX2*, *CDX1* and *CDX4* expression and the consequent decreased expression of posterior *HOX* genes, so that MNs adopt hindbrain rather than spinal identities.

At the current state of research, whether or not canonical WNT signaling is transduced by primary cilia remains controversial. Although some studies have demonstrated a localization of WNT signaling components in cilia or cilia proximity [123, 124] and a change in canonical WNT activity upon loss of cilia in certain cell types [125], other studies show that canonical WNT signaling functions independently of cilia [126]. Recently, it was shown that non-canonical WNT signaling via GSK-3β induces cilia formation in specific human cell lines [101]. Moreover, Rpgrip1l regulates non-canonical WNT signaling via preventing dishevelled degradation, thereby modulating planar cell polarity processes (PCP) [29]. Since WT and RPGRIP1L-deficient organoids are incubated at early stages of the differentiation protocol by the GSK-3β inhibitor CHIR99021 to activate WNT signaling and induce axial fate, it is most probable that WNT downregulation in the RPGRIP1L-deficient organoids takes

place downstream of GSK-3β. Therefore, the absence of primary cilia on axial progenitors might impact canonical and/or non-canonical WNT signaling, leading to the observed reduction in axial fate specification and the switch of MNs towards cervical/hindbrain identity instead of a thoracic spinal identity. In support of this hypothesis, no striking antero-posterior patterning defect was observed in TMEM67-deficient organoids, in which primary cilia were present on axial progenitors.

Further analyses will show how cilia regulate WNT signaling and consequently *CDX* and *HOX* gene expression during axial progenitor fate specification, or whether other pathways such as FGF and RA are implemented.

Relevance to the clinical features of ciliopathy patients

MNs play a pivotal role in human development. During prenatal life, their absence or degeneration, for instance in type 0 spinal muscular atrophy (SMA), generates a defect of fetal movements which eventually leads to malposition of joints (Fetal Akinesia Sequence, FAS) [127, 128]. To the best of our knowledge, FAS has never been reported in case of JS whatever the gene involved [11-13, 129]. Also, no evidence of ventral patterning defects or clinical signs of spinal motor dysfunction have been reported in the rare spinal cord descriptions in JS cases [32, 33].

Since the antero-posterior patterning defect of MNs described here most likely lead to a shift of boundaries between the posterior hindbrain region and the anterior spinal region with an increase in anterior identities, a corresponding phenotype could be present in ciliopathy patients. However, this shift might not lead to obvious defects or investigable symptoms in patients. Nevertheless, our study provides interesting entry points for further investigations where it will be important to analyze antero-posterior patterning more carefully and in additional CNS regions such as the hindbrain, as it is highly sensitive to antero-posterior patterning defects and one of the major targets of neurodevelopmental ciliopathies. Here, the increased expression of PHOX2B appears to be particularly interesting.

In humans, mutations in *PHOX2B* are the leading cause of the congenital central hypoventilation syndrome (CCHS), a rare genetic disorder of the nervous system involved in respiratory control [130], whereby PHOX2B is expressed in various neurons, including neurons of hindbrain structures such as the retrotrapezoid nucleus (RTN) and part of the medulla. Mutations of *Phox2b* in mice lead to severe hypoventilation and loss of the RTN [131, 132]. Interestingly, selective activation of the RTN region in rats induced increased ventilation [133, 134], demonstrating that the RTN is sensitive in both directions. In JS patients, a phenotype of effortless hyperventilation characterized by episodic tachypnea and/or apnea can be observed [135]. In general, this phenotype is variable, but was reported for JS patients with underlying *RPGRIP1L* as well as *TMEM67* mutations [12, 13, 129, 136-138]. Based on our findings of shifted antero-posterior patterning and increased numbers of PHOX2B+ neurons in a TZ gene mutant, we hypothesize that this defect affects hindbrain specificity in JS patients. Consequently, an increased number of PHOX2B+ neurons in the hindbrain could lead to overspecialisation and activation of the RTN. Unfortunately, there is no information on PHOX2B+ RTN in JS patients to date.

Our study thus calls for further analysis of the RTN in JS patients and of spinal and hindbrain antero-posterior patterning in JS patient-derived organoids.

Material and Methods

Generation of mESCs lines

Rpgrip1l$^{-/-}$ and *Rpgrip1l*$^{+/+}$ mouse ES cell lines were derived from blastocysts according to standard procedures [139] using *Ftm*-deficient mice produced and genotyped as described previously [15], and maintained in the C57BL/6J background. One ES clone from each genotype was used in this study.

mESCs culture and differentiation into ventral spinal organoids

mESCs were cultured in DMEM-GlutaMAX (Gibco) supplemented with 15% FCS, 100 µM β-mercaptoethanol, 100 U/ml penicillin, 0.1 mg/ml streptomycin, and 10^3 U/ml LIF (Millipore). To generate mouse spinal organoids, low-passage (inferior to 10) mESCs were dissociated and differentiated into embryoid bodies by seeding them in ultra-low attachment petri dishes (Corning) at a density of 9×10^4 cells ml^{-1} in N2B27 differentiation medium containing Advanced DMEMF12 and Neurobasal media (1:1, Life Technologies), B27 w/o vitamin A (Life Technologies), N2 (Life Technologies), 2 mM L-glutamine (Life Technologies), 0.1 mM β-mercaptoethanol, penicillin and streptomycin (Life Technologies). On day 2, the medium was changed and supplemented with 3µM CHIR, 10nM RA and 500nM SAG to induce ventral spinal fate. The medium was changed daily, with addition of 10nM RA only.

hiPSCs culture

hiPSCs were thawed in presence of Rock-inhibitor Y-27632 (5µM, Stemgent-Ozyme #04-0012) and cultured under standard conditions at 37°C in mTeSR+ medium (Stem Cell Technologies #100-0276) on Matrigel (Corning, VWR #354277) coated plates upon confluency of 70-80%. Passaging was performed using ReLeSR (Stem Cell Technologies #05872) and testing for potential mycoplasma contamination was performed regularly by Eurofins genomic (Mycoplasmacheck). Accutase (Stem Cell Technologies #07920) was used for the dissociation of hiPSC colonies into single cells.

Generation of mutant hiPSC lines

RPGRIP1L mutant and wildtype hiPSC clones were produced from two different hiPSC lines (PCIi033-A and UCSFi001-A) using CRISPR/Cas9 gene editing. The targeted exon 3 of *RPGRIP1L* and flanking sequences were sequenced prior to gene editing in both cell lines (see *on- and off-target analyses* section). The gRNA targeting exon 3 of *RPGRIP1L* was designed using the online design tool CRISPOR (134). Annealing of crRNA (Alt-R® CRISPR-Cas9 crRNA, 400 nM, IDT) and tracrRNA (Alt-R® CRISPR-Cas9 tracrRNA, 400 nM, IDT #1072533) was performed and 400.000 hiPSCs of each line were transfected with 1µl Cas9 protein (30 µM; kindly provided by TACGENE, Paris, France) and 1µl gRNA (200 µM) using nucleofection. The transfected cells were cultured in mTeSR+ medium (Stem Cell Technologies #100-0276) containing Rock-inhibitor Y-27632 (10 µM, Stemgent-Ozyme

#04-0012) for one day, replaced by mTeSR+ medium without Rock-inhibitor. Medium was changed every second day and serial dilutions were performed in mTeSR+ medium containing Rock-inhibitor Y-27632 and CloneR (1:1000, Stem Cell Technologies #05889). Rock-inhibitor was removed after two days and the medium containing CloneR was changed every second day until colonies were ready to be picked. Colonies were isolated in 24-well plates in mTesR+ medium containing CloneR. DNA was isolated for genotype analyses (see *on- and off-target analyses* section). Four WT (two clones of each hiPSC line) and four homozygous mutant hiPSC clones (two of each hiPSC line) carrying *InDel* mutations that lead to premature STOP were used for further analyses (Figure S2).

A large deletion of *RPGRIP1L* was induced in the PCli033-A line by combining the gRNA targeting exon 3 of *RPGRIP1L* with a gRNA targeting exon 27 of *RPGRIP1L* (Δexon3-exon27). This approach was performed at the ICV-iPS platform of the Brain Institute in Paris (ICM, Paris) under supervision of Stéphanie Bigou. One *RPGRIP1L KO* clone and one heterozygous control clone were used for further analyses (Figure S3). For the generation of TMEM67-deficient hiPSC clones from the PCli033-A cell line, the following strategy was used: The gRNA targeting exon 1 of *TMEM67* was combined with a gRNA targeting exon 27 of *TMEM67* to generate a large deletion of TMEM67 (Δexon1-exon27). One *TMEM67 KO* clone and one heterozygous control clone were used for further analyses (Figure S5). For all clones, genomic stability was assessed by detection of recurrent genetic abnormalities using the iCS-digitalTM PSC test, provided as a service by Stem Genomics (https://www.stemgenomics.com), as described previously [140].

On- and off-target analyses

Genomic DNA was extracted from both hiPSC lines (PCli033-A and UCSFi001-A) prior to CRISPR/Cas9 gene editing. Genotyping of on-targets was performed by PCR, and PCR products were sent for sequencing. After CRISPR/Cas9 gene editing, genomic DNA was isolated from individual hiPSC clones and the on-target sites were amplified by PCR. The PCR products were sent for sequencing to determine the specific mutations that were induced. Off-targets were identified using the CRISPOR online design tool [141] and ranked according to their CFD off-target score [142]. Potential off-targets within exons and with CFD scores > 0.02 [143] were selected for PCR and subsequent sequencing analyses. The primers used for on- and off-target analyses are listed in Table S1.

Differentiation of hiPSCs into spinal organoids

Differentiation of wildtype and RPGRIP1L mutant hiPSCs was performed as previously described [56, 57]. After amplification, hiPSC lines were dissociated into single cells using Accutase (Stem Cell Technologies #07920) and resuspended in differentiation medium N2B27 [vol:vol; Advanced DMEM/F-12 (Gibco) and Neurobasal Medium (Gibco)] supplemented with N2 (Thermo Fisher #17502048), B27 without Vitamin A (Thermo Fisher #12587010), penicillin/streptomycin 1 % (Thermo Fisher #15140122), β-mercaptoethanol 0.1 % (Thermo Fisher #31350010). Cells were seeded

in ultra-low attachment dishes (Corning #3261) to allow EB formation. The N2B27 differentiation medium was used throughout the whole differentiation process, but different additives were given at different time points (Figure 3A). Rock-inhibitor Y-27632 (5 µM; Stemgent-Ozyme #04-0012) was added from day 0 to day 2, CHIR-99021 (3 µM; Stemgent-Ozyme #04-0004) from day 0 to day 4, SB431542 (20 µM; Stemgent-Ozyme #04-0010) from day 0 to day 3 and LDN 193189 (0.1 µM; Stemgent-Ozyme #04-0074) from day 0 to day 4. The differentiation was preceded by adding Smoothened AGonist (SAG 500 nM; Merck #566660) and Retinoic Acid (100 nM RA; Sigma #R2625) to the N2B27 differentiation medium from day 4 to day 9. γ-Secretase inhibitor DAPT (10 µM; Tocris Bioscience #2634) was added from day 9 to the end of differentiation. Medium was changed every other day and additionally at day 3 of differentiation.

EB embedding and Cryosectioning

Murine and human spinal organoids were collected at different time points during differentiation, rinsed with PBS and fixed in cold PFA (4 %) for 7-12 min at 4 °C. EBs were rinsed in PBS and incubated in 30 % sucrose in PBS until completely saturated. Cryoprotected EBs were embedded in OCT embedding matrix (Cell Path #KMA-0100-00A) and stored at -80 °C. 12 µM cryostat sections were prepared and stored at -80 °C.

Immunofluorescence

Cryostat sections of murine and human EBs were washed in PBS/0.1% Triton X-100. Optional steps for permeabilization with PBS/0.5 %Triton X-100 for 10 min, post-fixation with MeOH (100 %) for 10 min or antigen-retrieval with Citrate-Buffer were performed depending on the antibody and specimen. After washing, cryosections were incubated with a blocking solution containing 10 % NGS in PBS/0.1% Triton-X100 for at least 2 hours. The sections were incubated with primary antibodies (Table S2) diluted in PBS/0.1 % Triton-X100 and 1 % NGS overnight at 4 °C. Next day, the slides were washed 3 x 5 min with PBS/0.1 % Triton-X100 and incubated with the secondary antibodies (Table S2) diluted in PBS/0.1 % Triton X-100 and 1 % NGS for 2 hours. After final washing steps with PBS/0.1 %Triton X-100 for at least 1 hour, sections were mounted with Vecta-Shield (Vector #H-1000) or Mowiol (Roth #0713.2) optionally containing DAPI (Merck #1.24653).

Image acquisition

Fluorescence image acquisition of patterning and differentiation markers was performed at room temperature using a Zeiss Observer Z1 equipped with an Apotome module, an Axiocam 506 monochrome cooled CCD camera and a 40x oil objective with a NA 1.3. All images were processed with Zen software (blue edition). Image analyses and figure preparation were performed using Fiji (ImageJ; National Institutes of Health). For cilia analyses, fluorescence images were acquired at room temperature using an inverted confocal microscope (LSM 710, Carl Zeiss AG or TCS SP5, Leica), a

63x oil objective with a NA 1.4, and a monochrome charge-coupled device camera. Z-stacks with 0.2 µM steps were acquired. Images were processed with Zen software (black edition). Image analyses and figure preparation were performed using Fiji (ImageJ; National Institutes of Health).

STED images were acquired on the STEDYCON confocal and STED module (Abberior Instruments GmbH, Germany) connected to the lateral port of an IX83 inverted microscope (Evident Scientific). The STEDYCON SmartControl software was used for data acquisition. Imaging was performed using a UPLXAPO 100x oil immersion objective (Evident Scientific). For STED, a pulsed 775 nm laser was used. STAR RED was excited with a pulsed 640 nm laser, STAR ORANGE was excited with a pulsed 561 nm laser, and DAPI was excited using a continuous wave 405nm source. Pixel size was 20 nm in xy direction, with a 250 nm step size in the z direction.

Quantification of fluorescent staining and statistical analyses

Fluorescent staining and protein band intensities were quantified using Fiji (ImageJ; National Institutes of Health). Intensity measurements of ciliary proteins were performed on unprocessed images (raw data) as described before [17, 23, 24, 27, 28]. After quantifications were performed, representative images were processed by means of background subtraction and contrast settings via Adobe Photoshop CS2.

For quantitative analyses of nuclear stainings, positive areas were defined and measured via manually setting thresholds in Fiji. For each image, the DAPI positive area (area 1) was determined and measured. The area 2 corresponding to the marker of interest was determined and measured, too. By dividing area 2 by area 1, the percentage of the positive area for each marker of interest per organoid slice was determined. At least 10 images per clone, from 2 independent experiments of differentiation were used for area quantifications.

All data are presented as mean ± SEM. Two-tailed t test with Welch's correction was performed for all data in which two datasets were compared. Two-tailed *t* test Analysis of variance (ANOVA) and Tukey honest significance difference (HSD) tests were used for all data in which more than two datasets were compared. Following statistical significances were considered: $*P < 0.05$, $**P < 0.01$, $***P < 0.001$ and $****P < 0.0001$. All statistical data analysis and graph illustrations were performed using GraphPad Prism (GraphPad Software).

RNA isolation and qPCR analyses

mESC- and hiPSC-derived organoids were collected at different stages during differentiation and washed with PBS. Material from one control (*TMEM67*$^{+/-}$) and one mutant (*TMEM67*$^{-/-}$) clone of the Ph2 hiPSC line was collected. RNA was isolated using the RNeasy Kit (Qiagen #74104) and RNAse-free DNase Set (Qiagen #79254). Isolated RNA was transcribed into cDNA using the GoScript Reverse Transcriptase Kit (Promega #A5001). For quantitative real-time PCR, 50 ng of cDNA of each sample was used in a Maxima SYBR Green/ROX qPCR Master Mix 2x (Thermo Scientific #K0222). Triplicate

reactions for each sample were prepared and the samples were run in a Step One Real-Time PCR System Thermal Cycling Block (Applied Biosystems #4376357). Primer pairs are listed in Table S1. The analysis of real-time data was performed using the included StepOne Software version 2.0 and graphs were generated using GraphPad Prism (GraphPad Software).

Bulk RNAseq analysis on mouse and human spinal organoids

mESC- and hiPSC-derived organoids were collected at different stages during differentiation and washed with PBS. For mouse organoids, samples from Wt and *Rpgrip1l* KO were collected from 3 independent experiments. For human organoids, material from two control clones of the Ph2 hiPSC line and the Wtc11 hiPSC line each (WT: n=4) and from one RPGRIP1L-deficient clone of the Ph2 hiPSC line and the Wtc11 hiPSC line each (KO: n=2) was collected. RNA was isolated using the RNeasy Kit (Qiagen #74104) and RNAse-free DNase Set (Qiagen #79254). RNA quality was determined by measuring the RNA integrity number (RIN) via the High Sensitive RNA Screen Tape Analysis kit (Agilent Technologies #5067) on the TapeStation system (Agilent Technologies). A RIN above 9.5 was considered as good quality RNA and 250 ng RNA in a total volume of 25 µl was prepared per sample for further procedure. Bulk RNAseq was realized by the Genotyping and Sequencing Core Facility of the Paris Brain Institute (iGenSeq, ICM Paris). RNAseq data processing was performed in Galaxy under supervision of the ARTBio platform (IBPS, Paris).

Paired-end RNA reads were aligned against the *M. musculus mm39* and the *homo sapiens hg38* genome, respectively, by using the STAR aligner (v2.7.10, Galaxy wrapper v4) [144] and the gene annotations gtf files GRCm39.109 and GRCh38.109, respectively. Quality of sequencing was controlled with fastQC (Galaxy wrapper v0.74+galaxy0) and MultiQC (Galaxy wrapper v1.11+galaxy1) [145]. Gene expression was assessed by counting sequencing reads aligned to gene exons with featureCounts (Galaxy wrapper v2.0.3+galaxy2) [146]. Raw counts were further converted to normalized gene expression values using the log2(tpm+1) transformation where tpm is the count of transcript aligned reads per length of transcript (kb) per million of total mapped reads (Galaxy tool "cpm_tpm_rpk" v0.5.2). Principal Component Analyses (PCA) were performed using r-factominer (v.2.9, Galaxy tool id "high_dimensions_visualisation" v4.3+galaxy0) [147] and heatmap visualizations were produced with the Galaxy tool "high_dim_heatmap" (v3.1.3+galaxy0) using the normalized gene expression values. Differentially expressed genes (DEGs) were selected from the gene raw read counts using DESeq2 (Galaxy wrapper v2.11.40.8+galaxy0) [148] and the Benjamini-Hochberg p-adjusted cutoff 0.01. DESeq2 statistical tables were used for generation of Volcano Plots (Galaxy tool id "volcanoplot" v0.0.5) [149], for goseq tests of overrepresented gene ontology categories (Galaxy wrapper v1.50.0+galaxy0) [150], as well as for Ensemble of Gene Set Enrichment Analyses (EGSEA) (Galaxy wrapper v1.20.0) [151].

Analysis of differential temporal profiles on human spinal organoids

We obtained 62710 gene temporal profiles of expression levels (expressed in log2(tpm+1), each composed of 7 time points in the WT and *RPGRIP1L* KO mutant contexts. We selected genes whose variance of expression across the 14 WT and KO time points is higher than 0.1, and we scaled each gene time point (WT and KO) using the minmax function on the TSPred R package, following which the scaled expression in each series is $E' = (E - E_{min}) / (E_{max} - E_{min})$, the highest expression of series is 1 and the lowest expression of series is 0. Note that since we scaled wild type and mutant expressions together, their relationship is maintained during the minmax scaling.

We next split the data into gene time series of 7 points in WT or KO context, and for each gene, we computed the euclidean distance between the wild type and mutant series. The density function of the euclidean distance was empirically derived from the observed distances. Using this function, we selected genes with the 1 % highest distances between time profiles in wild type or mutant context. Time profiles of selected genes were finally plotted using their unscaled expression values. Since the euclidean distance is not able to capture significant differences between all time series, we repeated the above analysis with 11 other distance metrics, including short time series (sts), dynamic time warping (dtw), time alignment measurement (tam), autocorrelation-based dissimilarity (acf), fourier discrete transform (fourier), compression-based dissimilarity (cdm), complexity-invariant (cid), Pearson's correlation dissimilarities (cor), integrated periodogram-based dissimilarity (int.per), periodogram-based dissimilarity (per) and Frechet (frechet) distances.

Gene time profiles selected using the various distances metrics are compiled in table [distance mode] which indicates for each gene the metrics that returned a significant distance. In total, we selected 542 genes with significant distance between mutant and wild-type time profiles. These profiles are sorted according to the number of metrics returning significant distance ($p < 0.01$). R code used for this analysis is available here for download.

Acknowledgement

Image acquisition was carried out at the IBPS Imaging Facility. We particularly thank Chloé Chaumeton from the IBPS imaging platform, and Frédéric Eghiaian from Abberior Instruments GmbH, for setting up the STED imaging system. We also thank the ICV-iPS platform at the Paris Brain Institute (ICM) for the generation and characterization of RPGRIP1L-deficient hiPSC lines, and the iGenSeq sequencing platform at the ICM for reliable sequencing and fast processing of our samples. We are very grateful to Vanessa Ribes and Pascal Gilardi Hebenstreit for providing us with protocols and help in mESCs culture and differentiation approaches. We also thank Jean-François Brunet for kindly providing the Phox2b antibody; and the TACGENE team of the Natural History Museum in Paris for providing the Cas9 protein. We thank Estelle Balissat for her help in the preparation of TMEM67 spinal cord organoids and cryosections. We also acknowledge the worldwide contributions of users and developers to the Galaxy project (https://galaxyproject.org/) and all the upstream authors and contributors of the software ecosystem we use and rely on.

This work was supported by funding to SSM from the *Fondation pour la Recherche Médicale* (Equipe FRM EQU201903007943), from the *Fondation pour la Recherche sur le Cancer* (ARC; PJA 20171206591), from the *Agence Nationale de la Recherche* (ANR; ERA-NET Neuron project on neurodevelopmental disorders “NDCil”). AW received funding from the *German Research Foundation* (DFG; WI 5451/1-1). ST received funding from the *Agence Nationale de la Recherche* (ANR; ANR-17-CE16-0003-01 and ANR-17-RHUS-0002).

Figure legends

Figure 1: Rpgrip1l-deficient mouse spinal progenitors fail to adopt SHH-dependent ventral fates. **(A)** Diagram depicting the main transcription factors spanning the different dorso-ventral progenitor (light blue) or neuronal (light green) domains of the developing spinal cord. FP: floor plate. p0-p2, pMN and p3 are ventral spinal progenitor domains. **(B)** Schematic summary of the spinal 3D differentiation approach. Main neural progenitor and neuron populations obtained at each time point with their molecular markers are indicated at the bottom. Small molecules used to induce or repress signaling pathways are indicated on top. CHIR: WNT agonist CHIR99021; SAG: SHH agonist; RA: Retinoic Acid. Modified after Maury et al., 2015 [56]. **(C)** Immunofluorescence for Olig2 (pMN) and Islet1 (post-mitotic MNs) in sections from Wt and *Rpgrip1l*$^{-/-}$ organoids at indicated time points. d: day of differentiation. **(D)** Immunofluorescence for Nkx6.1 (p3-pMN-p2), Olig2 (pMN), Nkx2.2 (p3), FoxA2 (FP) and Pax6 (pMN-dp) on sections from WT and *Rpgrip1l*$^{-/-}$ organoids at indicated time points. In C and D, nuclei are stained with DAPI. **(E, F, G, H)** Quantification of the relative areas stained for the indicated markers in sections from WT and *Rpgrip1l*$^{-/-}$ organoids at indicated time points. Data are shown as mean ± SEM. n sections analyzed ≧8, from ≧ 2 experimental replicates**. (I, J)** Heatmap depicting the average expression (log2(tpm+1)) of selected genes in WT and *Rpgrip1l-KO* spinal organoids over time. n=3 experimental replicates for each genotype. **(K)** Diagram depicting the ventral-to-dorsal switch in the types of spinal progenitors and neurons in *Rpgrip1l*$^{-/-}$ versus WT organoids. Data shown as mean ± SEM. ***P < 0.001, ****P < 0.0001 (unpaired t tests with Welch's correction). Scale bars: 50 µm.

Figure 2: Rpgrip1l-deficient mouse spinal organoids fail to activate the SHH pathway and lack functional cilia (A, B, C) Temporal analysis of *Gli1, Patched1 and Patched 2* expression in the course of the differentiation of WT and *Rpgrip1l*$^{-/-}$ organoids. Log2(tpm+1) data from bulk RNASeq analysis are displayed as mean ± SEM (n=3 for each genotype). **(D)** Immunofluorescence for the indicated ciliary markers on WT and Rpgrip1l-deficient spinal organoids at indicated time points. Cilia are present at apical sites pointing outside or into inner cavities of the organoids. **(E, F)** Quantifications of ciliary stainings. Data shown are mean ± SEM. n≧20 cilia from n≧3 organoids were analyzed per genotype. ***P < 0.001, ****P < 0.0001 (unpaired t tests with Welch's correction). Scale bar, 2 µm.

Figure 3: RPGRIP1L-deficient hiPSC-derived spinal organoids adopt the MN fate. (A) Schematic summary of the spinal 3D differentiation approach. Main neural progenitor and neuron populations obtained at each time point with their molecular markers are indicated at the bottom. Drugs used to induce or repress signaling pathways are indicated on top. SB and LDN: SMAD antagonists SB-431542 and LDN-193189; CHIR: WNT agonist CHIR99021; SAG: SHH agonist; DAPT: NOTCH agonist; RA: Retinoic Acid. Modified after Maury et al., 2015 [56]. **(B)** Immunofluorescence analysis of pMN

(OLIG2) and MN (ISLET1/2) production in WT and *RPGRIP1L*$^{-/-}$ spinal organoids. Scale bar: 50 µm. Quantifications show relative OLIG2 and ISLET1/2 positive areas per organoid over time. Data are shown as mean ± SEM. Asterisks denote statistical significance according to unpaired t tests with Welch's correction (*P < 0.05) (WT: n=4; KO: n=4). **(C)** Heatmap of selected gene expressions from bulk RNAseq data based on log2(tpm+1) values of WT and RPGRIP1L-deficient spinal organoids over time (WT: n=4; KO: n=2). (**C'**) Log2(tpm+1)-graphs illustrate the dynamic expression levels of *DBX2*, *OLIG2*, *NKX6.1* and *NKX2.2* in WT and *RPGRIP1L*$^{-/-}$ organoids. Data are shown as mean ± SEM (WT: n=4; KO: n=2). **(D)** Immunofluorescence analysis of OLIG2-positive MN progenitors and NKX2.2-positive spinal progenitors at day 9 and day 11. Scale bar: 50 µm. Data are shown as mean ± SEM. Asterisks denote statistical significance according to unpaired t tests with Welch's correction (*P < 0.05) (WT: n=4; KO: n=4). **(E)** Left: Immunofluorescence analysis of TUJ1 at day 14. Scale bar: 100 µm. Data are shown as mean ± SEM (WT: n=4; KO: n=4). Right: Log2(tpm+1) data from bulk RNASeq analyses show unaltered *TUJ1* expression between WT and RPGRIP1L-deficient organoids during differentiation. Data are shown as mean ± SEM (WT: n=4; KO: n=2).

Figure 4: RPGRIP1L-deficient hiPSC-derived neural progenitors harbor cilia and transduce SHH signaling. (A) Expression analysis of SHH target genes *GLI1* and *PTCH1*. Log2(tpm+1) data from bulk RNASeq analysis are displayed as mean ± SEM (WT: n=4; KO: n=2). **(B, C)** Immunofluorescence analysis of ciliary proteins in WT and RPGRIP1L-deficient spinal organoids at day 6. **(B)** Cilia are labeled by ARL13B in red and basal bodies by γ-TUBULIN in white. Scale bar: 300 µm. **(C)** Cilia are labeled by IFT81 in green. Scale bar: 1 µm. The graph shows unaltered ciliary length in *RGPRIP1L*$^{-/-}$ organoids compared to WT. Data are shown as mean ± SEM (WT: n=4; KO: n=4). **(D)** Stimulated-Emission-Depletion (STED) images of WT and RPGRIP1L-deficient cilia at day 6 of differentiation. Cilia are labeled by ARL13B in green. RPGRIP1L in red. Scale bar: 1 µm. Quantification of RPGRIP1L was measured on confocal images. Data are shown as mean ± SEM. Asterisks denote statistical significance according to unpaired t tests with Welch's correction (***P < 0.001) (WT: n=4; KO: n=4). **(E)** Immunofluorescence of WT and RPGRIP1L-deficient cilia on spinal organoids at day 6. Cilia are labeled by ARL13B in red and INPP5E in green. The basal body is labeled by γ-TUBULIN in white. Scale bar: 1 µM. Quantifications show an unaltered amount of INPP5E and a decreased amount of ARL13B in RPGRIP1L-deficient cilia. Data are shown as mean ± SEM. Asterisks denote statistical significance according to unpaired t tests with Welch's correction (***P < 0.001) (WT: n=4; KO: n=4). **(F)** Immunofluorescence of WT and RPGRIP1L-deficient cilia on spinal organoids at day 6. Cilia are labeled by ARL13B in green and AC3 in red. The basal body is labeled by γ-TUBULIN in white. Scale bar: 1 µm. Quantifications show a decreased amount of AC3 in RPGRIP1L-deficient cilia. Data are shown as mean ± SEM. Asterisks denote statistical significance according to unpaired t tests with Welch's correction (***P < 0.001) (WT: n=4; KO: n=4).

Figure 5: RPGRIP1L-deficient spinal organoids show anterior-posterior patterning defects with MNs adopting hindbrain identity. (A, B) Heatmaps showing **(A)** *HOXA* and **(B)** *HOXC* gene expression in WT and RPGRIP1L-deficient spinal organoids over time. The graphs were generated from log2(tpm+1) files of bulk RNASeq analysis (WT: n=4; KO: n=2). **(A', B')** Log2(tpm+1) graphs show the expression profiles of selected HOX genes *HOXA5*, *HOXA7*, *HOXC4* and *HOXC8* over time. Data are shown as mean ± SEM (WT: n=4; KO: n=2). **(C)** Immunofluorescence of WT and RPGRIP1L-deficient spinal organoids at day 14. HOXA5 is labeled in green and HOXC8 in red. Scale bar: 500 µm. Quantifications show the relative HOXA5 and HOXC8 positive areas per organoid. Data are shown as mean ± SEM. Asterisks denote statistical significance according unpaired t tests with Welch's correction (****P < 0.0001) (WT: n=4; KO: n=4). **(D)** Schematic overview about the four HOX gene clusters expressed from anterior to posterior positions. The black and red-dotted squares indicate the genes expressed in WT and RPGRIP1L-deficient spinal organoids, respectively. **(E, F)** Log2(tpm+1) graphs generated from bulk RNASeq analyses show the expression profiles of **(E)** *PHOX2B* and **(F)** *TBX20*. Data are shown as mean ± SEM (WT: n=4; KO: n=2). **(G)** Immunofluorescence of WT and RPGRIP1L-deficient spinal organoids at day 14. PHOX2B is labeled in green. Scale bar: 500 µm. Quantifications show the relative PHOX2B positive area per organoid. Data are shown as mean ± SEM. Asterisks denote statistical significance according unpaired t tests with Welch's correction (****P < 0.0001) (WT: n=4; KO: n=4).

Figure 6: Altered ciliogenesis on RPGRIP1L-deficient axial progenitors. (A-C) Log2(tpm+1) graphs generated from bulk RNASeq analyses show dynamic expression profiles of **(A)** *SOX2*, **(B)** *BRACHYURY* and **(C)** *CDX2*. Data are shown as mean ± SEM (WT: n=4; KO: n=2). **(D)** Immunofluorescence of WT and RPGRIP1L-deficient spinal organoids at day 2 and day 4. BRACHYURY is labeled in green. Scale bars: 250 µm. Quantifications show the relative BRACHYURY positive areas per organoid. Data are shown as mean ± SEM. Asterisks denote statistical significance according unpaired t tests with Welch's correction (****P < 0.0001) (WT: n=2; KO: n=2). **(E)** Immunofluorescence of WT and RPGRIP1L-deficient spinal organoids at day 4. CDX2 is stained in green. Scale bar: 250 µm. Quantifications show the relative CDX2 positive area per organoid. Data are shown as mean ± SEM (WT: n=2; KO: n=2). **(F, G)** Log2(tpm+1) graphs generated from bulk RNASeq analyses show dynamic expression profiles of **(F)** *CDX1* and **(G)** *CDX4*. Data are shown as mean ± SEM (WT: n=4; KO: n=2). **(H-J)** Immunofluorescence of cilia in WT and RPGRIP1L-deficient spinal organoids at **(H)** day 2 and **(I, J)** day 4. Cilia are labeled in green by ARL13B and in red by INPP5E (**H, I**) or in green by IFT81 and in red by ARL13B (**J**). Scale bars: 300 µm. Magnified areas are indicated by yellow rectangles and magnified images are displayed on the right. Scale bars: 5 µm.

Figure S1: Longitudinal transcriptomic analysis of WT and *Rpgrip1l*$^{-/-}$ spinal organoids. (A) Diagram depicting the time points of spinal differentiation chosen for bulk RNAseq analysis. **(B, C)** Temporal analysis of *Sox1* (NPs) and *Tuj1* (early neurons) in the course of the differentiation of WT and *Rpgrip1l*$^{-/-}$ organoids. Log2(tpm+1) data from bulk RNASeq analysis are displayed as mean ± SEM (n=3 for each genotype). **(D, E)** Ensemble of Gene Set Enrichment Analyses (*EGSEA*) at day 3 **(D)** and 4 **(E)** of the differentiation.

Figure S2: Generation of RPGRIP1L-deficient hiPSC lines. (A) Sequence of the CRISPR-guide that was used for the generation of mutations in exon 3 of *RPGRIP1L*. The Crispr Score corresponds to the CFD specificity score based on the CFD off-target model. The Off Target field indicates the number of off-targets for each number of mismatches (8 off-targets with 3 mismatches and 38 off-targets with 4 mismatches). None of these mismatches are in the 12 bp adjacent to the PAM. **(B)** List of hiPSC lines that were used in this project. The origin, clone number, genotype and specific mutation are indicated for each clone. **(C)** Immunofluorescence of RPGRIP1L in WT and RPGRIP1L-deficient cilia in spinal organoids at day 6 of differentiation. Cilia are labeled in red by ARL13B and RPGRIP1L is labeled in green. RPGRIP1L is detectable in WT but not RPGRIP1L-deficient cilia. **(D)** Identified off-targets and corresponding CFD scores for the *RPGRIP1L_exon3* guide. **(E)** Off-target analyses via sequencing of the *NPRL2* locus. Sequence of the CRISPR-guide is indicated above. Bases highlighted in yellow and green indicate mismatches between the guide sequence and the off-target sequence. No mutation in *NPRL2* was detectable around the off-target site in WT and KO hiPSC clones.

Figure S3: Full-deletion RPGRIP1L hiPSCs show no dorso-ventral but anterior-posterior specification defects during ventral spinal differentiations. (A) Sequences of the CRISPR-guides in exon 3 and exon 27 of *RPGRIP1L*, that were used for the generation of a full-deletion hiPSC line. The CRISPR Scores correspond to the CFD specificity scores based on the CFD off-target model. The Off Target field indicates the number of off-targets for each number of mismatches. None of these mismatches are in the 12 bp adjacent to the PAM. **(B)** hiPSC lines that were used in this project. The origin, clone number, genotype and specific mutation are indicated for both clones. **(C)** Immunofluorescence of RPGRIP1L in *RPGRIP1L*$^{+/-}$ and *RPGRIP1L*$^{-/-}$ spinal organoids at day 6. Cilia are labeled in red by ARL13B and RPGRIP1L in green. RPGRIP1L is detectable in RPGRIP1L$^{+/-}$ but not RPGRIP1L-deficient cilia. Scale bar: 2,5 µm. Quantifications show ciliary length and the relative ciliary RPGRIP1L amount. Data are shown as mean ± SEM. Asterisks denote statistical significance according unpaired t tests with Welch's correction (****P < 0.0001) (HET: n=1; KO: n=1). **(D)** Immunofluorescence analysis of MNs in *RPGRIP1L*$^{+/-}$ and *RPGRIP1L*$^{-/-}$ spinal organoids. Quantifications show the relative ISL1/2 positive area per organoid over time. Data are shown as mean ± SEM. Asterisks denote statistical significance according to unpaired t tests with Welch's correction (*P < 0.05) (WT: n=1; KO: n=1). **(E, F)** Immunofluorescence analysis of HOXA5 and HOXC8 in

RPGRIP1L$^{+/-}$ and *RPGRIP1L*$^{-/-}$ spinal organoids at day 14. Quantifications show relative **(E)** HOXA5 and **(F)** HOXC8 positive areas per organoid. Data are shown as mean ± SEM. Asterisks denote statistical significance according to unpaired t tests with Welch's correction (**P < 0.001; ****P < 0.0001) (WT: n=1; KO: n=1).

Figure S4: Patterning analyses in WT and RPGRIP1L-deficient ventral spinal organoids. (A) Immunofluorescence analysis of neural progenitors in WT and *RPGRIP1L*$^{-/-}$ spinal organoids at day 6. SOX2 and PAX6 are labeled in green. Quantifications show the relative SOX2 and PAX6 positive areas per organoid. Scale bar: 50 µm. Data are shown as mean ± SEM (WT: n=4; KO: n=4). **(B)** Immunofluorescence analysis of pMN in WT and *RPGRIP1L*$^{-/-}$ spinal organoids at day 9. NKX6.1 is stained in green and OLIG2 in red. Scale bar: 50 µm. Quantifications show relative NKX6.1 and OLIG2 positive areas per organoid. Data are shown as mean ± SEM (WT: n=4; KO: n=4). **(D, E)** Log2(tpm+1)-graphs shows dynamic expression levels of **(D)** *ISL1* and **(E)** *ISL2* in WT and *RPGRIP1L*$^{-/-}$ organoids. Data are shown as mean ± SEM (WT: n=4; KO: n=2). **(F)** Quantification of the number of NKX2.2-positive and NKX2.2/OLIG2 double-positive cells per organoid section for WT and RPGRIP1L-deficient spinal organoids at day 9 and day 11 (WT: n=4; KO: n=4). The number of double-positive cells is unaltered between WT and RPGRIP1L-deficient organoids. **(G)** Log2(tpm+1)-graph shows dynamic expression level of *MAP2* in WT and *RPGRIP1L*$^{-/-}$ organoids. Data are shown as mean ± SEM (WT: n=4; KO: n=2). **(H)** Immunofluorescence analysis of the ciliary GPR161 amount in WT and *RPGRIP1L*$^{-/-}$ spinal organoids at day 6. Organoids are either treated with SAG to stimulate SHH signaling or DMSO-treated as control. GPR161 is labeled in green and cilia are labeled in red via ARL13B. Quantifications show normalized GPR161 amounts within cilia. Scale bar: 2,5 µm. Data are shown as mean ± SEM (WT: n=4; KO: n=4).

Figure S5: Spinal differentiation of TMEM67-deficient hiPSC lines. (A) Sequences of the CRISPR-guides in exon 1 and exon 27, that were used for the generation of a full-deletion hiPSC line. The CRISPR Score corresponds to the CFD specificity score based on the CFD off-target model. The Off Target field indicates the number of off-targets for each number of mismatches. None of these mismatches are in the 12 bp adjacent to the PAM. **(B)** List of hiPSC lines that were used in this project. The origin, clone number, genotype and specific mutation are indicated for each clone. **(C)** Immunofluorescence of TMEM67 in *TMEM67*$^{+/-}$ and *TMEM67*$^{-/-}$ spinal organoids at day 6. Cilia are labeled in red by ARL13B and basal bodies in white by γ-TUBULIN. TMEM67 is labeled in green. Scale bar: 10 µm. Magnified areas are indicated by yellow rectangles and magnified images are displayed on the lower right. Scale bar: 1 µm. **(D, E)** Quantification of the ciliary TMEM67 amount **(D)** and ciliary length **(E)** in *TMEM67*$^{+/-}$ and *TMEM67*$^{-/-}$ spinal organoids at day 6. Data are shown as mean ± SEM. Asterisks denote statistical significance according to unpaired t tests with Welch's correction (****P < 0.0001) (WT: n=1; KO: n=1). **(F)** Immunofluorescence of primary cilia in

TMEM67$^{+/-}$ and *TMEM67*$^{-/-}$ spinal organoids. Cilia are labeled via INPP5E in green and γ-TUBULIN in red. Scale bar: 50 µm. Magnified areas are indicated by yellow rectangles and magnified images are displayed on the lower left. Scale bar: 2 µm. **(G, H, I)** qPCR analyses of **(G)** *GLI1*, **(H)** *PTCH1* and **(I)** *ISL1* gene expression profiles in *TMEM67*$^{+/-}$ and *TMEM67*$^{-/-}$ spinal organoids over time. Data are presented as mean ± SEM of technical replicates (HET: n=1; KO: n=1). **(J)** Immunofluorescence analysis of MNs in *TMEM67*$^{+/-}$ and *TMEM67*$^{-/-}$ spinal organoids at day 14. Scale bar: 75 µm. Quantification shows the relative ISL1/2 positive area per organoid. Data are shown as mean ± SEM (HET: n=1; KO: n=1; N=3).

Figure S6: Bulk RNAseq analysis indicates anterior-posterior patterning abnormalities in RPGRIP1L-deficient spinal organoids. (A) Schematic summary of the spinal 3D differentiation approach. Samples for bulk RNAseq analyses were collected at indicated time points (WT: n=4; KO: n=2). **(B)** PCA analyses performed on WT and KO samples show the variation of data over time. The zoom-in on the left shows that WT and KO samples cluster closely together at single time points. **(C, D)** Volcano plots of RNAseq data on day 11 **(C)** and day 14 **(D)**. The threshold for significance was set to 0.01 and the LogFC threshold to color to 2. **(E)** EGSEA at day 2 of spinal differentiation shows downregulated *anterior/posterior_pattern_specification* (GO:0009952) in RPGRIP1L-deficient organoids. **(F)** List of genes with different temporal expression profiles based on euclidean distance measurements between WT and KO organoids over the entire time course of differentiation. Asterisks indicate genes that are related to anterior-posterior patterning. **(G)** Examples of genes with different temporal expression profiles. *HOXC8* was captured via time alignment measurement (tam) and *HOXC9* via euclidean measurement.

Figure S7: Anterior-posterior patterning defects in RPGRIP1L-deficient spinal organoids. (A) Heatmap showing *HOXB* and *HOXD* gene expressions in WT and RPGRIP1L-deficient spinal organoids over time. The graph was generated from log2(tpm+1) files of bulk RNASeq analysis (WT: n=4; KO: n=2). **(B-G)** Log2(tpm+1) graphs show expression profiles of **(B)** *FGF8*, **(C)** *FGF3*, **(D)** *EGR2/KROX20*, **(E)** *PHOX2A*, **(F)** *NKX2.8/NKX2.9* and **(G)** *WNT5A* over time. Data are shown as mean ± SEM (WT: n=4; KO: n=2).

Figure S8: TMEM67-deficient spinal organoids display cilia on axial progenitors with MNs that show a mild shift in anterior-posterior patterning. (A, B) Immunofluorescence of cilia in *TMEM67*$^{+/-}$ and *TMEM67*$^{-/-}$ spinal organoids at day 4. Cilia are labeled by IFT81 in green and ARL13B in red **(A)** or by INPP5E in green and ARL13B in red **(B)**. Cilia are present at apical sites pointing into inner cavities of the organoids. Scale bar: 50 µm. **(A)** Magnified areas are indicated by yellow rectangles and magnified images are displayed in the middle. Scale bar: 5 µm. **(C)** Immunofluorescence of HOXC8 in *TMEM67*$^{+/-}$ and *TMEM67*$^{-/-}$ spinal organoids at day 14. Scale bar: 50 µm. Quantifications show the

relative HOXC8 positive areas per organoid. Data are shown as mean ± SEM (HET: n=1; KO n=1). Asterisks denote statistical significance according unpaired t tests with Welch's correction (* P < 0.05). **(D, E)** qPCR analyses of **(D)** *HOXC6* and **(E)** *HOXC9* gene expression profiles in *TMEM67*$^{+/-}$ and *TMEM67*$^{-/-}$ spinal organoids over time. Data are presented as mean ± SEM of technical replicates (HET n=1; KO: n=1). **(F)** Immunofluorescence of PHOX2B in *TMEM67*$^{+/-}$ and *TMEM67*$^{-/-}$ spinal organoids at day 14. Scale bar: 50 µm. Quantifications show the relative PHOX2B positive areas per organoid. Data are shown as mean ± SEM (HET: n=1; KO n=1; N=3). **(G)** qPCR analyses of *PHOX2B* gene expression profiles in *TMEM67*$^{+/-}$ and *TMEM67*$^{-/-}$ spinal organoids over time. Data are presented as mean ± SEM of technical replicates (HET n=1; KO: n=1).

Figure S9: Mouse Rpgrip1l-deficient spinal organoids do not display spinal to cranial specification defects. (A, B, C, D, E) Temporal analysis of *Cdx1, Cdx2, Cdx4* (spinal identity) *Cyp26a1* (cranial identity) and *Brachyury* (NMPs) expression in the course of the differentiation of WT and *Rpgrip1l*$^{-/-}$ organoids. Log2(tpm+1) data from bulk RNASeq analysis are displayed as mean ± SEM (n=3 for each genotype). **(F)** Immunofluorescence for Cdx2 on sections from WT and *Rpgrip1l*$^{-/-}$ organoids at day 4. **(G)** Quantification of the relative areas stained for Cdx2. Data are shown as mean ± SEM. n sections analyzed ≧6. **(H)** Heatmap depicting the average expression (log2(tpm+1) of selected *Hox* genes in WT and *Rpgrip1l-KO* spinal organoids over time. n=3 experimental replicates for each genotype. **(I)** Temporal analysis of *Hoxc10 and Hoxd10* in the course of the differentiation of WT and *Rpgrip1l*$^{-/-}$ organoids. Log2(tpm+1) data from bulk RNASeq analysis are displayed as mean ± SEM (n=3 for each genotype).

References

1. Bachmann-Gagescu, R., et al., *Healthcare recommendations for Joubert syndrome.* Am J Med Genet A., 2020. **182**(1): p. 229-249.
2. Reiter, J. and M. Leroux, *Genes and molecular pathways underpinning ciliopathies.* Nat. Rev. Mol. Cell Biol., 2017. **18**(9): p. 533-547.
3. Brancati, F., B. Dallapiccola, and E. Valente, *Joubert Syndrome and related disorders.* Orphanet J Rare Dis., 2010. **5**: p. 20.
4. Goetz, S. and K. Anderson, *The primary cilium: a signalling centre during vertebrate development.* Nat. Rev. Genet., 2010. **11**(5): p. 331-344.
5. Spassky, N., et al., *Primary cilia are required for cerebellar development and Shh-dependent expansion of progenitor pool.* Dev Biol., 2008. **317**(1): p. 246-259.
6. Andreu-Cervera, A., M. Catala, and S. Schneider-Maunoury, *Cilia, ciliopathies and hedgehog-related forebrain developmental disorders.* Neurobiol. Dis., 2021. **150**: p. 105236.
7. Andreu-Cervera, A., et al., *The ciliopathy gene ftm/rpgrip1l controls mouse forebrain patterning via region-specific modulation of hedgehog/gli signaling.* J. Neurosci., 2019. **39**(13): p. 2398-2415.
8. Abdelhamed, Z., et al., *The ciliary Frizzled-like receptor Tmem67 regulates canonical Wnt/β-catenin signalling in the developing cerebellum via Hoxb5.* Sci Rep., 2019. **9**(1): p. 5446.
9. Lancaster, M., et al., *Defective Wnt-dependent cerebellar midline fusion in a mouse model of Joubert syndrome.* Nat. Med., 2011. **17**(6): p. 726-731.
10. Basten, S. and R. Giles, *Functional aspects of primary cilia in signaling, cell cycle and tumorigenesis.* Cilia, 2013. **2**(1): p. 6.
11. Delous, M., et al., *The ciliary gene RPGRIP1L is mutated in cerebello-oculo-renal syndrome (Joubert syndrome type B) and Meckel syndrome.* Nat. Genet., 2007. **39**(7): p. 875-881.
12. Arts, H., et al., *Mutations in the gene encoding the basal body protein RPGRIP1L, a nephrocystin-4 interactor, cause Joubert syndrome.* Nat. Genet., 2007. **39**(7): p. 882-888.
13. Doherty, D., et al., *Mutations in 3 genes (MKS3, CC2D2A and RPGRIP1L) cause COACH syndrome (Joubert syndrome with congenital hepatic fibrosis).* J. Med. Genet., 2010. **47**(1): p. 8-21.
14. Wolf, M., et al., *Mutational analysis of the RPGRIP1L gene in patients with Joubert syndrome and nephronophthisis.* Kidney Int., 2007. **72**(12): p. 1520-1526.
15. Vierkotten, J., et al., *Ftm is a novel basal body protein of cilia involved in Shh signalling.* Development, 2007. **134**(14): p. 2569-2577.
16. Besse, L., et al., *Primary cilia control telencephalic patterning and morphogenesis via Gli3 proteolytic processing.* Development, 2011. **138**(10): p. 2079-2088.
17. Garcia-Gonzalo, F., et al., *A transition zone complex regulates mammalian ciliogenesis and ciliary membrane composition.* Nat. Genet., 2011. **43**(8): p. 776-784.
18. Li, C., et al., *MKS5 and CEP290 Dependent Assembly Pathway of the Ciliary Transition Zone.* PLoS Biol., 2016. **14**(3): p. e1002416.
19. Shi, X., et al., *Super-resolution microscopy reveals that disruption of ciliary transition-zone architecture causes Joubert syndrome.* Nat. Cell Biol., 2017. **19**(10): p. 1178-1188.
20. Benzing, T. and B. Schermer, *Transition zone proteins and cilia dynamics.* Nat. Genet., 2011. **43**(8): p. 723-724.
21. Reiter, J., O. Blacque, and M. Leroux, *The base of the cilium: roles for transition fibres and the transition zone in ciliary formation, maintenance and compartmentalization.* EMBO Rep., 2012. **13**(7): p. 608-618.
22. Williams, C., et al., *MKS and NPHP modules cooperate to establish basal body/transition zone membrane associations and ciliary gate function during ciliogenesis.* J. Cell Biol., 2011. **192**(6): p. 1023-1041.
23. Wiegering, A., et al., *Cell type-specific regulation of ciliary transition zone assembly in vertebrates.* EMBO J., 2018. **37**(10): p. e97791.
24. Wiegering, A., et al., *Rpgrip1l controls ciliary gating by ensuring the proper amount of Cep290 at the vertebrate transition zone.* Mol Biol Cell., 2021. **32**(8): p. 675-689.

25. Omran, H., *NPHP proteins: gatekeepers of the ciliary compartment.* J. Cell Biol., 2010. **190**(5): p. 715-717.
26. Sang, L., et al., *Mapping the NPHP-JBTS-MKS protein network reveals ciliopathy disease genes and pathways.* Cell, 2011. **145**(4): p. 513-528.
27. Gerhardt, C., et al., *The transition zone protein Rpgrip1l regulates proteasomal activity at the primary cilium.* J. Cell Biol., 2015. **210**(1): p. 115-133.
28. Struchtrup, A., et al., *The ciliary protein RPGRIP1L governs autophagy independently of its proteasome-regulating function at the ciliary base in mouse embryonic fibroblasts.* Autophagy, 2018. **14**(4): p. 567-583.
29. Mahuzier, A., et al., *Dishevelled stabilization by the ciliopathy protein Rpgrip1l is essential for planar cell polarity.* J. Cell Biol., 2012. **198**(5): p. 927-940.
30. Gerhardt, C., et al., *Control of Hedgehog signalling by the cilia-regulated proteasome.* J. Dev. Biol., 2016. **4**(3): p. 27.
31. Willaredt, M., et al., *A crucial role for primary cilia in cortical morphogenesis.* J Neurosci., 2008. **28**(48): p. 12887-12900. .
32. Juric-Sekhar, G., et al., *Joubert syndrome: brain and spinal cord malformations in genotyped cases and implications for neurodevelopmental functions of primary cilia.* Acta Neuropathol., 2012. **123**(5): p. 695-709.
33. ten Donkelaar, H., F. Hoevenaars, and P. Wesseling, *A case of Joubert's syndrome with extensive cerebral malformations.* Clin Neuropathol., 2000. **19**(2): p. 85-93.
34. Abdelhamed, Z., et al., *The Meckel-Gruber syndrome protein TMEM67 controls basal body positioning and epithelial branching morphogenesis in mice via the non-canonical Wnt pathway.* Dis Model Mech., 2015. **8**(6): p. 527-541.
35. Abdelhamed, Z., et al., *Variable expressivity of ciliopathy neurological phenotypes that encompass Meckel-Gruber syndrome and Joubert syndrome is caused by complex de-regulated ciliogenesis, Shh and Wnt signalling defects.* Hum Mol Genet., 2013. **22**(7): p. 1358-1372.
36. Adams, M., et al., *A meckelin–filamin A interaction mediates ciliogenesis.* Hum. Mol. Genet., 2012. **21**: p. 1272–1286.
37. Briscoe, J. and J. Ericson, *Specification of neuronal fates in the ventral neural tube.* J. Curr Opin Neurobiol., 2001. **11**(1): p. 43-49.
38. Bangs, F. and K. Anderson, *Primary Cilia and Mammalian Hedgehog Signaling.* Cold Spring Harb. Perspect. Biol., 2017. **9**(5): p. pii: a028175.
39. Balaskas, N., et al., *Gene regulatory logic for reading the Sonic Hedgehog signaling gradient in the vertebrate neural tube.* Cell, 2012. **148**(1-2): p. 273-284. .
40. Ribes, V., et al., *Distinct Sonic Hedgehog signaling dynamics specify floor plate and ventral neuronal progenitors in the vertebrate neural tube.* Genes Dev., 2010. **24**(11): p. 1186-1200.
41. Dessaud, E., et al., *Dynamic assignment and maintenance of positional identity in the ventral neural tube by the morphogen sonic hedgehog.* PLoS Biol., 2010. **8**(6): p. e1000382.
42. Dessaud, E., et al., *Interpretation of the sonic hedgehog morphogen gradient by a temporal adaptation mechanism.* Nature, 2007. **450**(7170): p. 717-720.
43. Jeong, J. and A. McMahon, *Growth and pattern of the mammalian neural tube are governed by partially overlapping feedback activities of the hedgehog antagonists patched 1 and Hhip1.* Development, 2005. **132**(1): p. 143-154.
44. Lek, M., et al., *A homeodomain feedback circuit underlies step-function interpretation of a Shh morphogen gradient during ventral neural patterning.* Development, 2010. **137**(23): p. 4051-4060.
45. Huangfu, D., et al., *Hedgehog signalling in the mouse requires intraflagellar transport proteins.* Nature, 2003. **426**(6962): p. 83-87.
46. Huangfu, D. and K. Anderson, *Cilia and Hedgehog responsiveness in the mouse.* Proc Natl Acad Sci U S A. , 2005. **102**(32): p. 11325-11330.
47. Haycraft, C., et al., *Gli2 and Gli3 localize to cilia and require the intraflagellar transport protein polaris for processing and function.* PLoS Genet., 2005. **1**(4): p. e53.
48. Liu, A., B. Wang, and L. Niswander, *Mouse intraflagellar transport proteins regulate both the activator and repressor functions of Gli transcription factors.* Development, 2005. **132**(13): p. 3103-3111.

49. Wichterle, H., et al., *Directed differentiation of embryonic stem cells into motor neurons.* Cell, 2002. **110**(3): p. 385-397.
50. Duval, N., et al., *BMP4 patterns Smad activity and generates stereotyped cell fate organization in spinal organoids.* Development, 2019. **146**(14): p. dev175430.
51. Catala, M., M. Teillet, and N. Le Douarin, *Organization and development of the tail bud analyzed with the quail-chick chimaera system.* Mech Dev., 1995. **51**(1): p. 51-65.
52. Wymeersch, F., et al., *Position-dependent plasticity of distinct progenitor types in the primitive streak.* Elife, 2016. **5**: p. e10042.
53. Wymeersch, F., V. Wilson, and A. Tsakiridis, *Understanding axial progenitor biology in vivo and in vitro.* Development, 2021. **148**(4): p. dev180612.
54. Cambray, N. and V. Wilson, *Two distinct sources for a population of maturing axial progenitors. Development.* Development., 2007. **134**(15): p. 2829-2840.
55. Cambray, N. and V. Wilson, *Axial progenitors with extensive potency are localised to the mouse chordoneural hinge.* Development, 2002. **129**(20): p. 4855-4866.
56. Maury, Y., et al., *Combinatorial analysis of developmental cues efficiently converts human pluripotent stem cells into multiple neuronal subtypes.* Nature Biotechnology, 2015. **33**(1): p. 89-96.
57. Mouilleau, V., et al., *Dynamic extrinsic pacing of the HOX clock in human axial progenitors controls motor neuron subtype specification.* Development, 2021. **146**(6): p. dev194514.
58. Jang, S., E. Gunmit, and H. Wichterle, *Human-specific progenitor sub-domain contributes to extended neurogenesis and increased motor neuron production.* bioRxiv, 2022.
59. Briscoe, J., et al., *Homeobox gene Nkx2.2 and specification of neuronal identity by graded Sonic hedgehog signalling.* Nature, 1999. **398**(6728): p. 622-627. .
60. Jensen, V., et al., *Formation of the transition zone by Mks5/Rpgrip1L establishes a ciliary zone of exclusion (CIZE) that compartmentalises ciliary signalling proteins and controls PIP2 ciliary abundance.* EMBO J., 2015. **34**(20): p. 2537-2556.
61. Garcia-Gonzalo, F., et al., *Phosphoinositides Regulate Ciliary Protein Trafficking to Modulate Hedgehog Signaling.* Dev. Cell, 2015. **34**(4): p. 400-409.
62. Mukhopadhyay, S., et al., *The ciliary G-protein-coupled receptor Gpr161 negatively regulates the Sonic hedgehog pathway via cAMP signaling.* Cell, 2013. **152**(1-2): p. 210-223.
63. Pal, K., et al., *Smoothened determines β-arrestin-mediated removal of the G protein-coupled receptor Gpr161 from the primary cilium.* J Cell Biol., 2016. **212**(7): p. 861-875.
64. Chen, C., et al., *Ciliopathy protein HYLS1 coordinates the biogenesis and signaling of primary cilia by activating the ciliary lipid kinase PIPKIγ.* Sci Adv., 2021. **7**(26): p. eabe3401. .
65. Dasen, J., J. Liu, and T. Jessell, *Motor neuron columnar fate imposed by sequential phases of Hox-c activity.* Nature, 2003. **425**(6961): p. 926-933.
66. Deschamps, J. and D. Duboule, *Embryonic timing, axial stem cells, chromatin dynamics, and the Hox clock.* Genes Dev., 2017. **31**(14): p. 1406-1416.
67. Liu, J., E. Laufer, and T. Jessell, *Assigning the positional identity of spinal motor neurons: rostrocaudal patterning of Hox-c expression by FGFs, Gdf11, and retinoids.* Neuron, 2001. **32**(6): p. 997-1012.
68. Pattyn, A., et al., *Control of hindbrain motor neuron differentiation by the homeobox gene Phox2b.* Development, 2000. **127**(2): p. 1349-1358. .
69. Ahn, D., et al., *tbx20, a new vertebrate T-box gene expressed in the cranial motor neurons and developing cardiovascular structures in zebrafish.* Mech Dev., 2000. **95**(1-2): p. 253-258.
70. Pattyn, A., et al., *Coordinated temporal and spatial control of motor neuron and serotonergic neuron generation from a common pool of CNS progenitors.* Genes Dev., 2003. **17**(6): p. 729-737.
71. Jarrar, W., et al., *Nkx2.2 and Nkx2.9 are the key regulators to determine cell fate of branchial and visceral motor neurons in caudal hindbrain.* PloS One, 2015. **10**(4): p. e0124408.
72. Guthrie, S., *Patterning and axon guidance of cranial motor neurons.* Nat Rev Neurosci., 2007. **8**(1): p. 859-871. .
73. Seitanidou, T., et al., *Krox-20 is a key regulator of rhombomere-specific gene expression in the developing hindbrain.* Mechanisms of Development, 1997. **65**: p. 31-42.

74. Schneider-Maunoury, S., P. Gilardi-Hebenstreit, and P. Charnay, *How to build a vertebrate hindbrain. Lessons from genetics.* C R Acad Sci III., 1998. **321**(10): p. 819-834. .
75. Frank, D. and D. Sela-Donenfeld, *Hindbrain induction and patterning during early vertebrate development.* Cell Mol Life Sci., 2019. **76**(5): p. 941-960.
76. Aragon, F. and C. Pujades, *FGF signaling controls caudal hindbrain specification through Ras-ERK1/2 pathway.* BMC Dev Biol., 2009. **9**(61).
77. Walshe, J., et al., *Establishment of hindbrain segmental identity requires signaling by FGF3 and FGF8.* Curr Biol., 2002. **12**(13): p. 1117-1123.
78. Hirsch, M., et al., *Forced expression of Phox2 homeodomain transcription factors induces a branchio-visceromotor axonal phenotype.* Dev Biol., 2007. **303**(2): p. 687-702.
79. Andre, P., et al., *Wnt5a and Wnt11 regulate mammalian anterior-posterior axis elongation.* Development, 2015. **142**(8): p. 1516-1527.
80. Forlani, S., K. Lawson, and J. Deschamps, *Acquisition of Hox codes during gastrulation and axial elongation in the mouse embryo.* Development, 2003. **130**(16): p. 3807-3819.
81. Gouti, M., et al., *A Gene Regulatory Network Balances Neural and Mesoderm Specification during Vertebrate Trunk Development.* Dev Cell., 2017. **41**(3): p. 243-261.e7.
82. Henrique, D., et al., *Neuromesodermal progenitors and the making of the spinal cord.* Development, 2015. **142**(17): p. 2864-2875. .
83. Kondoh, H., S. Takada, and T. Takemoto, *Axial level-dependent molecular and cellular mechanisms underlying the genesis of the embryonic neural plate.* Dev Growth Differ., 2016. **58**(5): p. 427-436.
84. Wymeersch, F., et al., *Transcriptionally dynamic progenitor populations organised around a stable niche drive axial patterning.* Development, 2019. **146**(1): p. dev168161.
85. Nordström, U., et al., *An early role for WNT signaling in specifying neural patterns of Cdx and Hox gene expression and motor neuron subtype identity.* PLoS Biol., 2006. **4**(8): p. e252.
86. van den Akker, E., et al., *Cdx1 and Cdx2 have overlapping functions in anteroposterior patterning and posterior axis elongation.* Development, 2002. **129**(9): p. 2181-2193.
87. Marom, K., E. Shapira, and A. Fainsod, *The chicken caudal genes establish an anterior-posterior gradient by partially overlapping temporal and spatial patterns of expression.* Mech Dev., 1997. **64**(1-2): p. 41-52.
88. Metzis, V., et al., *Nervous System Regionalization Entails Axial Allocation before Neural Differentiation.* Cell, 2018. **175**(4): p. 1105-1118.e17.
89. Chang, J., I. Skromne, and R. Ho, *CDX4 and retinoic acid interact to position the hindbrain-spinal cord transition.* Dev Biol., 2016. **410**(2): p. 178-189.
90. Sturgeon, K., et al., *Cdx1 refines positional identity of the vertebrate hindbrain by directly repressing Mafb expression.* Development, 2011. **138**(1): p. 65-74.
91. Skromne, I., et al., *Repression of the hindbrain developmental program by Cdx factors is required for the specification of the vertebrate spinal cord.* Development, 2007. **134**(11): p. 2147-2158.
92. Joshi, P., A. Darr, and I. Skromne, *CDX4 regulates the progression of neural maturation in the spinal cord.* Dev Biol., 2019. **449**(2): p. 132-142.
93. De Mori, R., et al., *Joubert syndrome-derived induced pluripotent stem cells show altered neuronal differentiation in vitro.* Cell Tissue Res., 2024. **396**(2): p. 255-267.
94. Bangs, F., et al., *Lineage specificity of primary cilia in the mouse embryo.* Nat Cell Biol., 2015. **17**(2): p. 113-22.
95. Soares, H., et al., *Cilia Distal Domain: Diversity in Evolutionarily Conserved Structures.* Cells, 2019. **8**(2): p. 160.
96. Wang, J., et al., *Variable phenotypes and penetrance between and within different zebrafish ciliary transition zone mutants.* Dis Model Mech., 2022. **15**(12): p. dmm049568.
97. Chang, C., et al., *Atoh1 Controls Primary Cilia Formation to Allow for SHH-Triggered Granule Neuron Progenitor Proliferation.* Developmental Cell, 2019. **48**(2): p. 184-199.
98. Ong, T., et al., *Siah2 integrates mitogenic and extracellular matrix signals linking neuronal progenitor ciliogenesis with germinal zone occupancy.* Nat Commun., 2020. **11**(1): p. 5312.
99. Blaess, S., et al., *Beta1-integrins are critical for cerebellar granule cell precursor proliferation.* J Neurosci., 2004. **24**(13): p. 3402-3412.

100. Akhshi, T. and W. Trimble, *A non-canonical Hedgehog pathway initiates ciliogenesis and autophagy.* J Cell Biol. , 2021. **220**(1): p. e202004179.
101. Zhang, K., et al., *Primary cilia are WNT-transducing organelles whose biogenesis is controlled by a WNT-PP1 axis.* 2023. **58**(2): p. 139-154.e8.
102. Lippmann, E., et al., *Deterministic HOX patterning in human pluripotent stem cell-derived neuroectoderm.* Stem Cell Reports, 2015. **14**(4): p. 632-644.
103. Miller, A. and J. Dasen, *Establishing and maintaining Hox profiles during spinal cord development.* Semin Cell Dev Biol., 2024. **152-153**: p. 44-57.
104. Afzal, Z. and R. Krumlauf, *Transcriptional Regulation and Implications for Controlling Hox Gene Expression.* J Dev Biol., 2022. **10**(1): p. 4.
105. Cooper, F., et al., *Notch signalling influences cell fate decisions and HOX gene induction in axial progenitors.* Development, 2024. **151**(3): p. dev202098.
106. Wind, M., et al., *Defining the signalling determinants of a posterior ventral spinal cord identity in human neuromesodermal progenitor derivatives.* Development, 2021. **148**(6): p. dev194415.
107. Young, T. and J. Deschamps, *Hox, Cdx, and anteroposterior patterning in the mouse embryo.* J. Curr Top Dev Biol., 2009. **88**: p. 235-255.
108. Takada, S., et al., *Wnt-3a regulates somite and tailbud formation in the mouse embryo.* Genes Dev., 1994. **8**(2): p. 174-189.
109. Subramanian, V., B. Meyer, and P. Gruss, *Disruption of the murine homeobox gene Cdx1 affects axial skeletal identities by altering the mesodermal expression domains of Hox genes.* Cell, 1995. **83**(4): p. 641-653.
110. Chawengsaksophak, K., et al., *Cdx2 is essential for axial elongation in mouse development.* Proc Natl Acad Sci U S A., 2004. **101**(20): p. 7641-7645.
111. van Nes, J., et al., *The Cdx4 mutation affects axial development and reveals an essential role of Cdx genes in the ontogenesis of the placental labyrinth in mice.* Development, 2006. **133**(3): p. 419-428.
112. Davidson, A. and L. Zon, *The caudal-related homeobox genes cdx1a and cdx4 act redundantly to regulate hox gene expression and the formation of putative hematopoietic stem cells during zebrafish embryogenesis.* Dev Biol., 2006. **292**(2): p. 506-518.
113. Faas, L. and H. Isaacs, *Overlapping functions of Cdx1, Cdx2, and Cdx4 in the development of the amphibian Xenopus tropicalis.* Dev Dyn., 2009. **238**(4): p. 835-852.
114. Epstein, M., et al., *Patterning of the embryo along the anterior-posterior axis: the role of the caudal genes.* Development, 1997. **124**(19): p. 3805-3814.
115. Pownall, M., et al., *eFGF, Xcad3 and Hox genes form a molecular pathway that establishes the anteroposterior axis in Xenopus.* Development, 1996. **122**(12): p. 3881-3892.
116. Gogolou, A., et al., *Early anteroposterior regionalisation of human neural crest is shaped by a pro-mesodermal factor.* Elife, 2022. **11**: p. e74263.
117. Amin, S., et al., *Cdx and T Brachyury Co-activate Growth Signaling in the Embryonic Axial Progenitor Niche.* Cell Rep., 2016. **17**(12): p. 3165-3177.
118. Neijts, R., et al., *Cdx is crucial for the timing mechanism driving colinear Hox activation and defines a trunk segment in the Hox cluster topology.* Dev Biol., 2017. **422**(2): p. 146-154.
119. Mazzoni, E., et al., *Saltatory remodeling of Hox chromatin in response to rostrocaudal patterning signals.* Nature Neurosci., 2013. **16**(9): p. 1191-1198.
120. Young, T., et al., *Cdx and Hox genes differentially regulate posterior axial growth in mammalian embryos.* Dev Cell., 2009. **17**(4): p. 516-526.
121. Pilon, N., et al., *Cdx4 is a direct target of the canonical Wnt pathway.* Dev Biol., 2006. **289**(1): p. 55-63.
122. Schyr, R., et al., *Cdx1 is essential for the initiation of HoxC8 expression during early embryogenesis.* FASEB J., 2012. **26**(6): p. 2674-2684.
123. Simons, M., et al., *Inversin, the gene product mutated in nephronophthisis type II, functions as a molecular switch between Wnt signaling pathways.* Nat Genet., 2005. **37**(5): p. 537-543.
124. Veland, I., et al., *Inversin/Nephrocystin-2 is required for fibroblast polarity and directional cell migration.* PLoS One, 2013. **8**(4): p. e60193.
125. Lancaster, M., J. Schroth, and J. Gleeson, *Subcellular spatial regulation of canonical Wnt signalling at the primary cilium.* Nat Cell Biol., 2011. **13**(6): p. 700-707.

126. Ocbina, P., M. Tuson, and K. Anderson, *Primary cilia are not required for normal canonical Wnt signaling in the mouse embryo.* PLoS One, 2009. **4**(8): p. e6839.
127. Niles, K., et al., *Fetal arthrogryposis multiplex congenita/fetal akinesia deformation sequence (FADS)-Aetiology, diagnosis, and management.* Prenat Diagn., 2019. **39**(9): p. 720-731.
128. Grotto, S., et al., *Type 0 Spinal Muscular Atrophy: Further Delineation of Prenatal and Postnatal Features in 16 Patients.* J Neuromuscul Dis, 2016. **3**(4): p. 487-495.
129. Brancati, F., et al., *RPGRIP1L mutations are mainly associated with the cerebello-renal phenotype of Joubert syndrome-related disorders.* Clin. Genet., 2008. **74**(2): p. 164-170.
130. Bishara, J., T. Keens, and I. Perez, *The genetics of congenital central hypoventilation syndrome: clinical implications.* Appl Clin Genet., 2018. **11**: p. 135-144.
131. Dubreuil, V., et al., *A human mutation in Phox2b causes lack of CO2 chemosensitivity, fatal central apnea, and specific loss of parafacial neurons.* Proc Natl Acad Sci U S A., 2008. **105**(3): p. 1067-1072.
132. Dubreuil, V., et al., *Defective respiratory rhythmogenesis and loss of central chemosensitivity in Phox2b mutants targeting retrotrapezoid nucleus neurons.* J Neurosci., 2009. **29**(47): p. 14836-14846.
133. Li, A. and E. Nattie, *CO2 dialysis in one chemoreceptor site, the RTN: stimulus intensity and sensitivity in the awake rat.* Respir Physiol Neurobiol., 2002. **133**(1-2): p. 11-22.
134. Kanbar, R., et al., *Photostimulation of Phox2b medullary neurons activates cardiorespiratory function in conscious rats.* Am J Respir Crit Care Med., 2010. **182**(9): p. 1184-1194.
135. Joubert, M., et al., *Familial agenesis of the cerebellar vermis. A syndrome of episodic hyperpnea, abnormal eye movements, ataxia, and retardation.* Neurology, 1969. **19**(9): p. 813-825.
136. Brancati, F., et al., *MKS3/TMEM67 mutations are a major cause of COACH Syndrome, a Joubert Syndrome related disorder with liver involvement.* Hum Mutat., 2009. **30**(2): p. E432-442.
137. Baala, L., et al., *The Meckel-Gruber syndrome gene, MKS3, is mutated in Joubert syndrome.* Am J Hum Genet., 2007. **80**(1): p. 186-194.
138. Kroes, H., et al., *Joubert syndrome: genotyping a Northern European patient cohort.* Eur J Hum Genet., 2016. **24**(2): p. 214-220.
139. Bernex, F., et al., *Spatial and temporal patterns of c-kit-expressing cells in WlacZ/+ and WlacZ/WlacZ mouse embryos.* Development, 1996. **122**(10): p. 3023-3033.
140. Assou, S., et al., *Recurrent Genetic Abnormalities in Human Pluripotent Stem Cells: Definition and Routine Detection in Culture Supernatant by Targeted Droplet Digital PCR.* Stem Cell Reports, 2020. **14**(1): p. 1-8.
141. Concordet, J. and M. Haeussler, *CRISPOR: intuitive guide selection for CRISPR/Cas9 genome editing experiments and screens.* Nucleic Acids Res., 2018. **26**(W1): p. W242-W245. .
142. Doench, J., et al., *Optimized sgRNA design to maximize activity and minimize off-target effects of CRISPR-Cas9.* Nat Biotechnol., 2016. **34**(2): p. 184-191.
143. Haeussler, M., et al., *Evaluation of off-target and on-target scoring algorithms and integration into the guide RNA selection tool CRISPOR.* Genome Biol., 2016. **17**(1): p. 148.
144. Dobin, A., et al., *STAR: ultrafast universal RNA-seq aligner.* Bioinformatics., 2013. **29**(1): p. 15-21.
145. Ewels, P., et al., *MultiQC: summarize analysis results for multiple tools and samples in a single report.* Bioinformatics., 2016. **32**(19): p. 3047-48.
146. Liao, Y., G. Smyth, and W. Shi, *featureCounts: an efficient general purpose program for assigning sequence reads to genomic features.* Bioinformatics., 2014. **30**(7): p. 923-930.
147. Lê, S., J. Josse, and F. Husson, *FactoMineR: An R Package for Multivariate Analysis.* Journal of Statistical Software, 2008. **25**(1): p. 1-18.
148. Love, M., W. Huber, and S. Anders, *Moderated estimation of fold change and dispersion for RNA-seq data with DESeq2.* Genome Biol., 2014. **15**(12): p. 550.
149. Zink, R., R. Wolfinger, and G. Mann, *Summarizing the incidence of adverse events using volcano plots and time intervals.* Clin Trials., 2013. **10**(3): p. 398-406.
150. Young, M., et al., *Gene ontology analysis for RNA-seq: accounting for selection bias.* Genome Biol., 2010. **11**(2): p. R14.
151. Alhamdoosh, M., et al., *Combining multiple tools outperforms individual methods in gene set enrichment analyses.* Bioinformatics., 2017. **33**(3): p. 414-424.

Figure 1

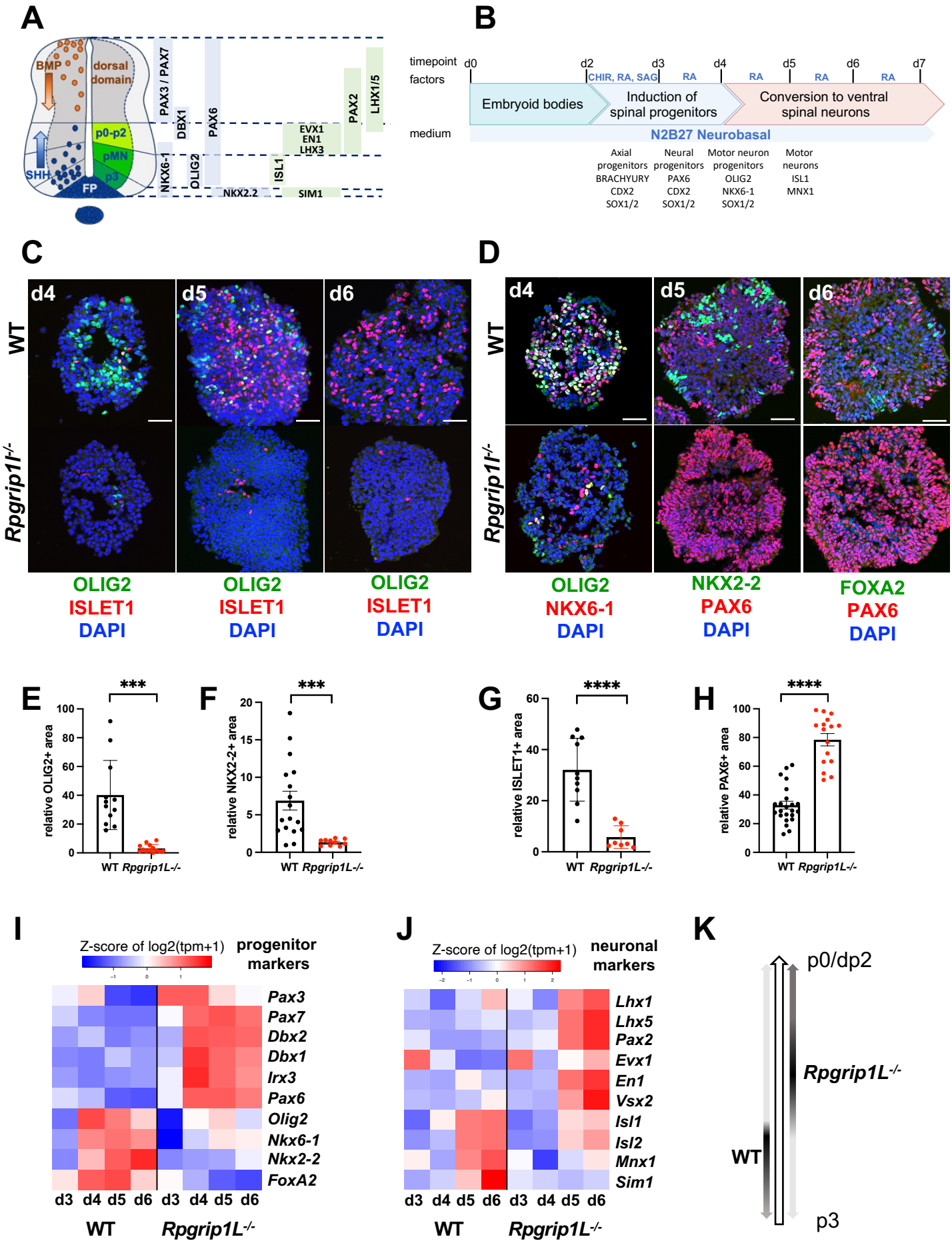
A
BMP
dorsal domain
p0-p2
pMN
p3
FP
SHH
PAX3 / PAX7
DBX1
PAX6
PAX2
LHX1/5
EVX1
EN1
LHX3
NKX6-1
OLIG2
ISL1
NKX2.2
SIM1
B
timepoint
factors
medium
d0
d2
d3
d4
d5
d6
d7
CHIR, RA, SAG
RA
Embryoid bodies
Induction of spinal progenitors
Conversion to ventral spinal neurons
N2B27 Neurobasal
Axial progenitors BRACHYURY CDX2 SOX1/2
Neural progenitors PAX6 CDX2 SOX1/2
Motor neuron progenitors OLIG2 NKX6-1 SOX1/2
Motor neurons ISL1 MNX1
C
D
WT
Rpgrip1l-/-
d4
d5
d6
OLIG2
ISLET1
DAPI
NKX6-1
NKX2-2
PAX6
FOXA2
E
F
G
H
relative OLIG2+ area
relative NKX2-2+ area
relative ISLET1+ area
relative PAX6+ area
***
****
WT
Rpgrip1L-/-
I
J
K
Z-score of log2(tpm+1)
progenitor markers
neuronal markers
Pax3
Pax7
Dbx2
Dbx1
Irx3
Pax6
Olig2
Nkx6-1
Nkx2-2
FoxA2
Lhx1
Lhx5
Pax2
Evx1
En1
Vsx2
Isl1
Isl2
Mnx1
Sim1
d3 d4 d5 d6 d3 d4 d5 d6
p0/dp2
p3

Figure 2

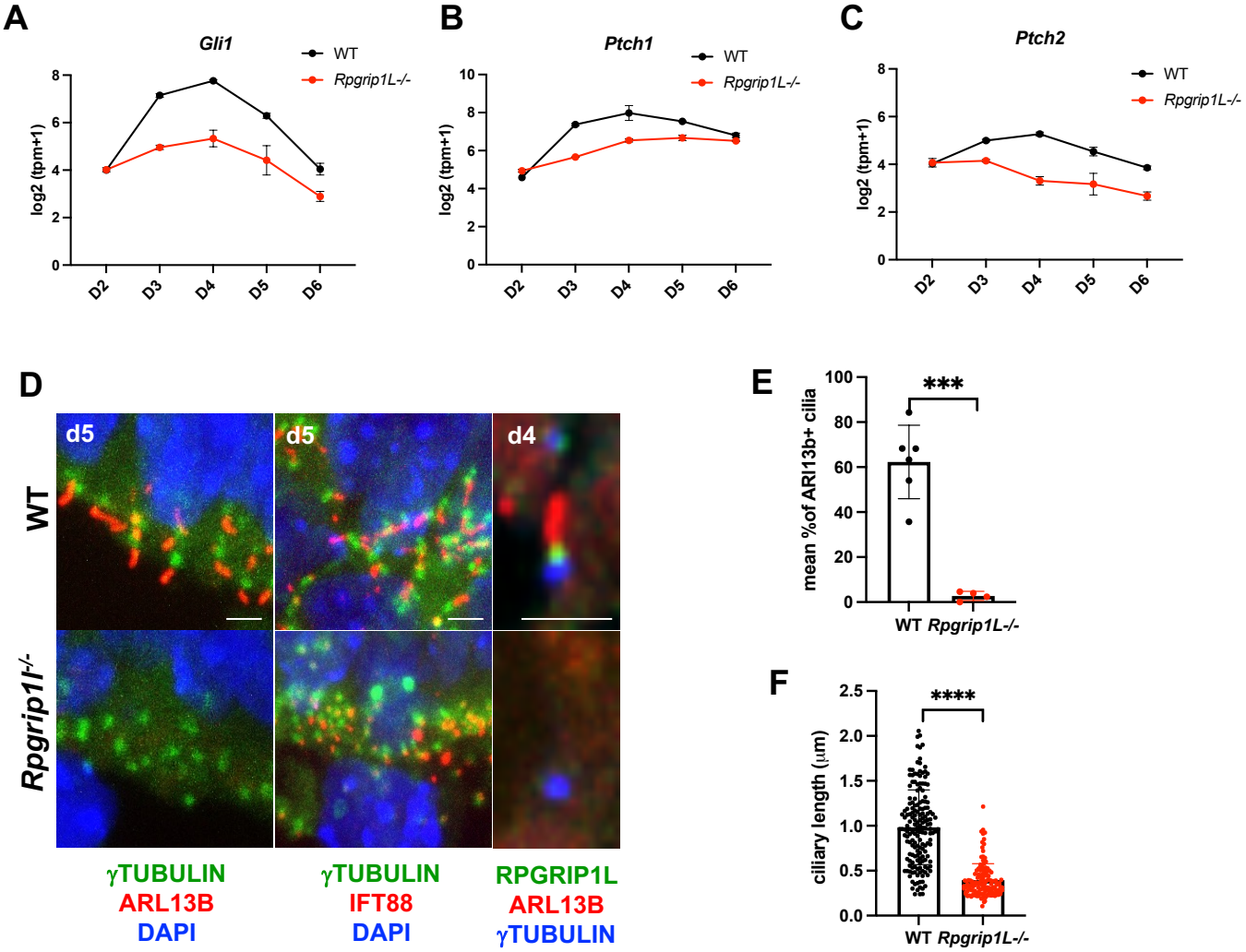
A
Gli1
WT
Rpgrip1L-/-
log2 (tpm+1)
D2
D3
D4
D5
D6
B
Ptch1
C
Ptch2
D
WT
Rpgrip1l-/-
d5
d5
d4
γTUBULIN
ARL13B
DAPI
γTUBULIN
IFT88
DAPI
RPGRIP1L
ARL13B
γTUBULIN
E
mean %of ARl13b+ cilia
***
WT
Rpgrip1L-/-
F
ciliary length (μm)
****
WT
Rpgrip1L-/-

Figure 3

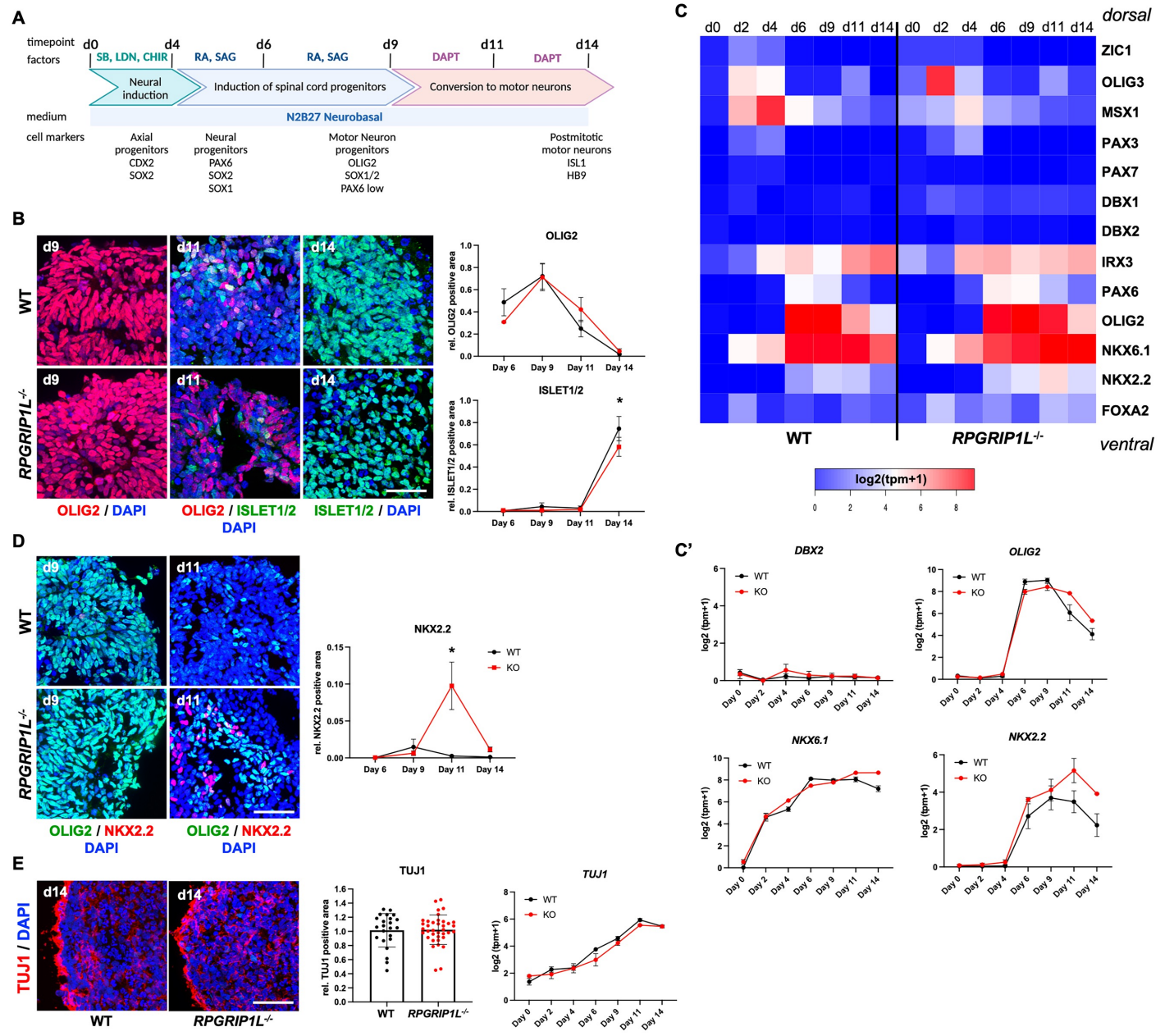
A
timepoint
factors
d0
d4
d6
d9
d11
d14
SB, LDN, CHIR
RA, SAG
RA, SAG
DAPT
DAPT
Neural induction
Induction of spinal cord progenitors
Conversion to motor neurons
medium
N2B27 Neurobasal
cell markers
Axial progenitors CDX2 SOX2
Neural progenitors PAX6 SOX2 SOX1
Motor Neuron progenitors OLIG2 SOX1/2 PAX6 low
Postmitotic motor neurons ISL1 HB9
B
WT
RPGRIP1L-/-
d9
d11
d14
OLIG2 / DAPI
OLIG2 / ISLET1/2 DAPI
ISLET1/2 / DAPI
OLIG2
rel. OLIG2 positive area
ISLET1/2
rel. ISLET1/2 positive area
Day 6
Day 9
Day 11
Day 14
C
dorsal
ventral
d0 d2 d4 d6 d9 d11 d14
ZIC1
OLIG3
MSX1
PAX3
PAX7
DBX1
DBX2
IRX3
PAX6
OLIG2
NKX6.1
NKX2.2
FOXA2
WT
RPGRIP1L-/-
log2(tpm+1)
C'
DBX2
OLIG2
NKX6.1
NKX2.2
WT
KO
log2 (tpm+1)
D
WT
RPGRIP1L-/-
d9
d11
OLIG2 / NKX2.2 DAPI
NKX2.2
rel. NKX2.2 positive area
E
TUJ1 / DAPI
d14
WT
RPGRIP1L-/-
TUJ1
rel. TUJ1 positive area

Figure 4

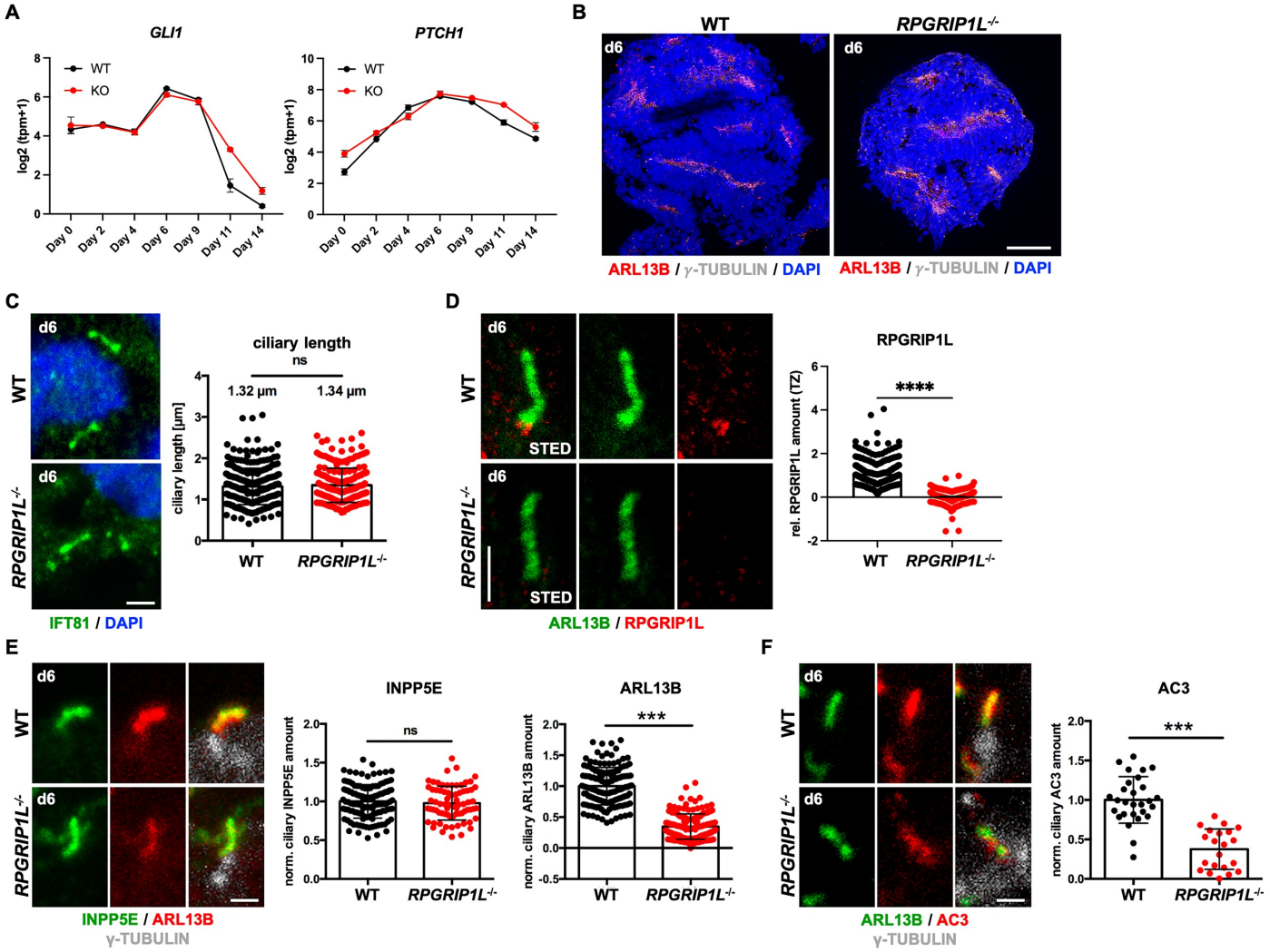
A
GLI1
PTCH1
WT
KO
log2 (tpm+1)
Day 0
Day 2
Day 4
Day 6
Day 9
Day 11
Day 14
B
WT
RPGRIP1L-/-
d6
ARL13B / γ-TUBULIN / DAPI
C
d6
WT
RPGRIP1L-/-
IFT81 / DAPI
ciliary length
ns
1.32 µm
1.34 µm
ciliary length [µm]
D
STED
RPGRIP1L
****
rel. RPGRIP1L amount (TZ)
ARL13B / RPGRIP1L
E
INPP5E
ARL13B
ns
***
norm. ciliary INPP5E amount
norm. ciliary ARL13B amount
INPP5E / ARL13B
γ-TUBULIN
F
AC3
norm. ciliary AC3 amount
ARL13B / AC3
γ-TUBULIN

Figure 5

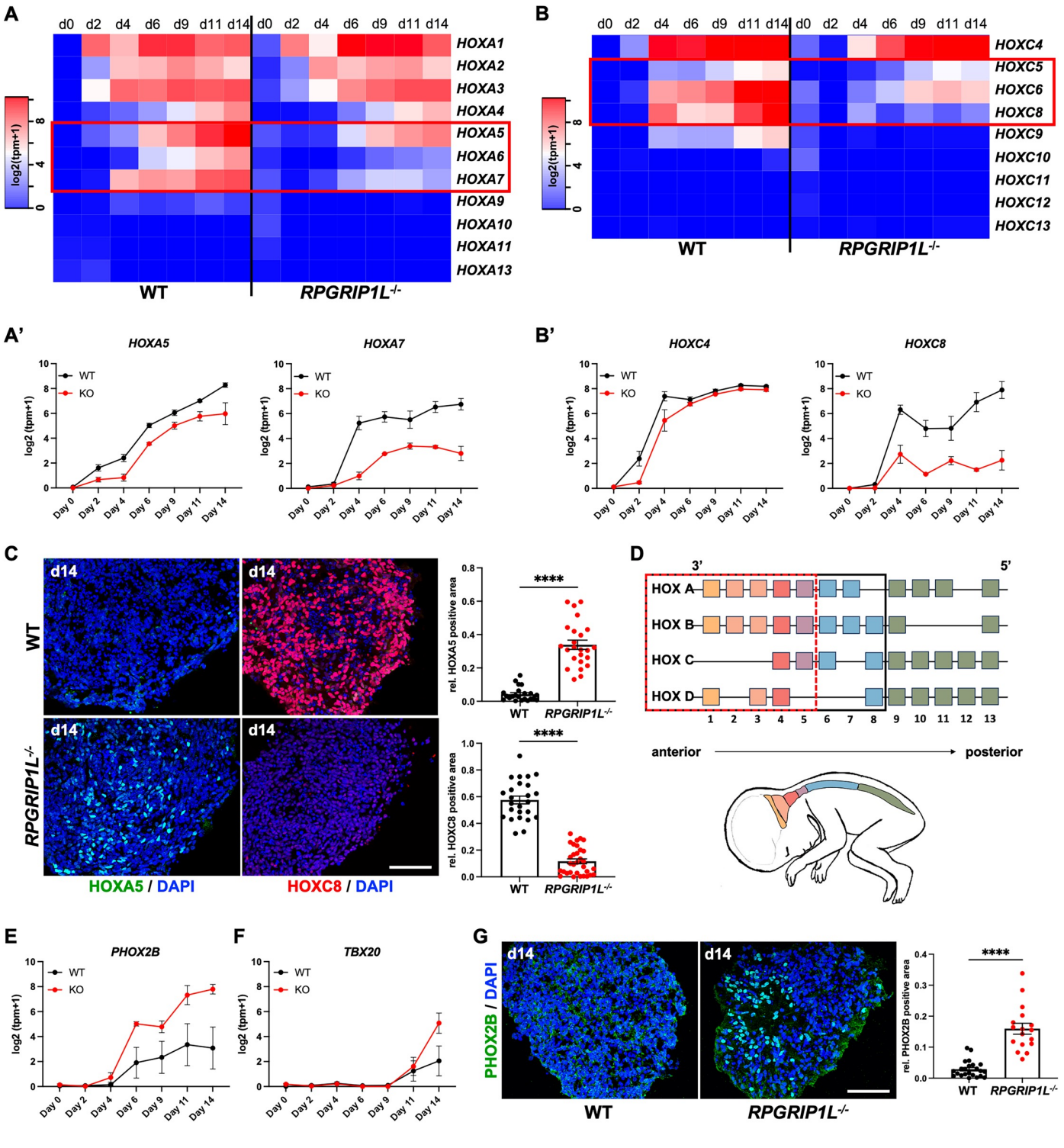
A
d0 d2 d4 d6 d9 d11 d14 d0 d2 d4 d6 d9 d11 d14
HOXA1
HOXA2
HOXA3
HOXA4
HOXA5
HOXA6
HOXA7
HOXA9
HOXA10
HOXA11
HOXA13
log2(tpm+1)
WT
RPGRIP1L-/-
B
HOXC4
HOXC5
HOXC6
HOXC8
HOXC9
HOXC10
HOXC11
HOXC12
HOXC13
A'
HOXA5
HOXA7
B'
HOXC4
HOXC8
WT
KO
log2 (tpm+1)
Day 0 Day 2 Day 4 Day 6 Day 9 Day 11 Day 14
C
d14
HOXA5 / DAPI
HOXC8 / DAPI
rel. HOXA5 positive area
rel. HOXC8 positive area
****
D
3'
5'
HOX A
HOX B
HOX C
HOX D
anterior
posterior
E
PHOX2B
F
TBX20
G
PHOX2B / DAPI
rel. PHOX2B positive area

Figure 6

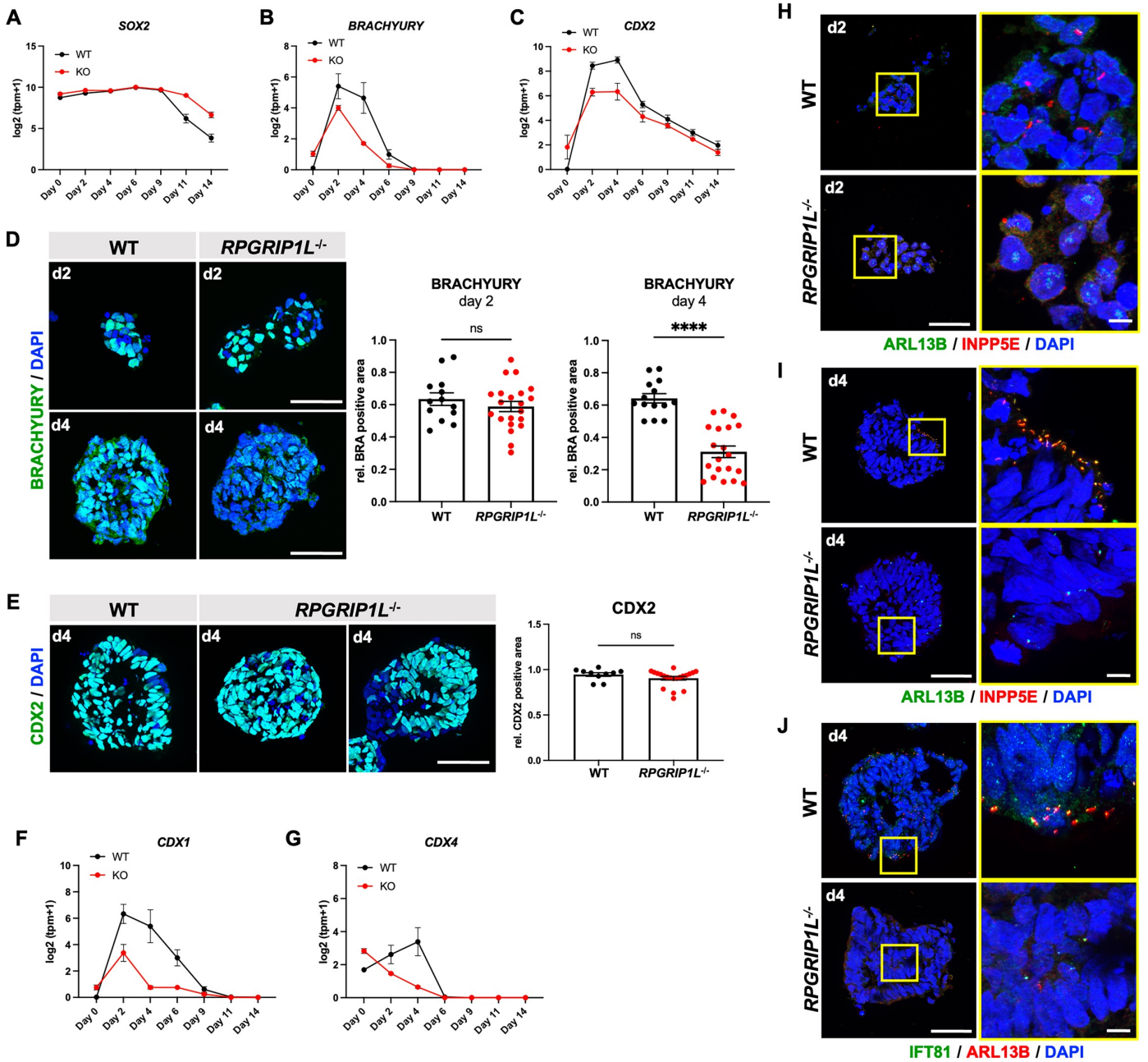
A
SOX2
B
BRACHYURY
C
CDX2
WT
KO
log2 (tpm+1)
Day 0
Day 2
Day 4
Day 6
Day 9
Day 11
Day 14
D
WT
RPGRIP1L-/-
d2
d4
BRACHYURY / DAPI
BRACHYURY
day 2
ns
BRACHYURY
day 4
****
rel. BRA positive area
E
CDX2 / DAPI
CDX2
rel. CDX2 positive area
F
CDX1
G
CDX4
H
ARL13B / INPP5E / DAPI
I
ARL13B / INPP5E / DAPI
J
IFT81 / ARL13B / DAPI

Figure S1

A

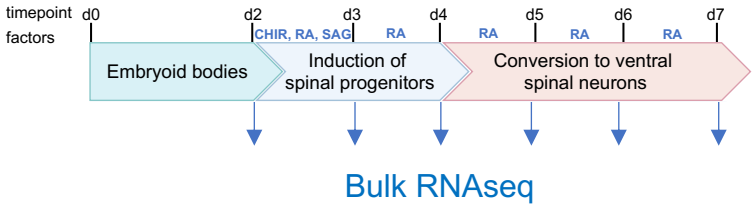

B

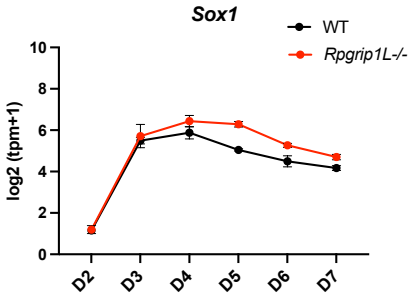

C

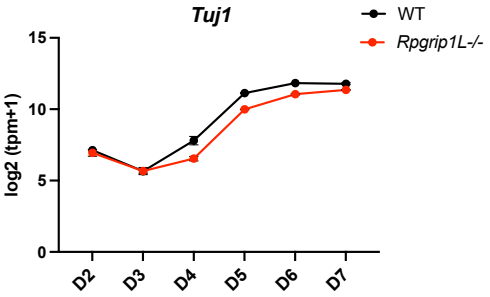

D

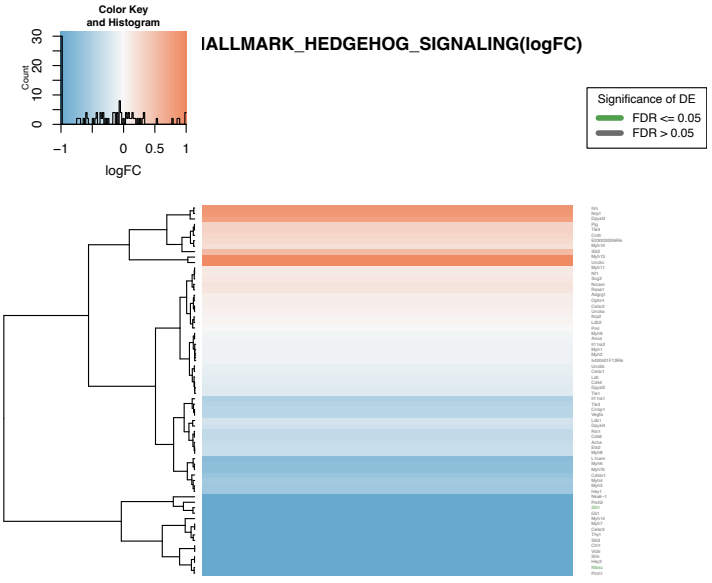

E

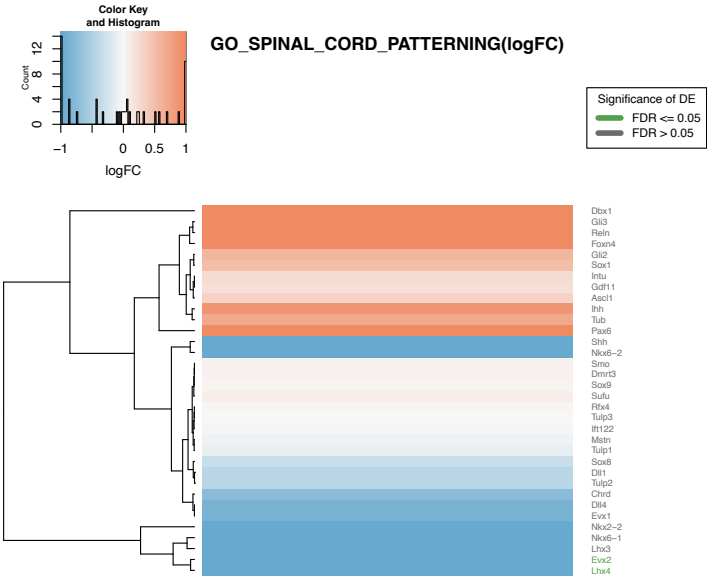

Figure S2

A

Guide	Sequence + PAM	Crispr Score	Off Target
RPGRIP1L_exon3	ACGGACAATGAAGTCTCGCC AGG	92	0-0-0-8-38

B

Cell line	Origin	# clone	Genotype	Method	Mutation
Ph2	PCli033-A	42	+/+	InDel	-
Ph2	PCli033-A	46	+/+	InDel	-
Ph2	PCli033-A	20	-/-	InDel	c.114_118del; p.Arg39Glyfs*8 c.116del; p.Arg39Profs*44
Ph2	PCli033-A	44	-/-	InDel	c.115dup; p.Arg39Profs*10 c.115dup; p.Arg39Profs*10
Wtc11	UCSFi001-A	19	+/+	InDel	-
Wtc11	UCSFi001-A	62	+/+	InDel	-
Wtc11	UCSFi001-A	44	-/-	InDel	c.114_115insG; p.Arg39Alafs*10 c.116_117delinsT; p.Arg39Leufs*44
Wtc11	UCSFi001-A	65	-/-	InDel	c.114_115dup; p.Arg39Leufs*45 c.114_115dup; p.Arg39Leufs*45

C

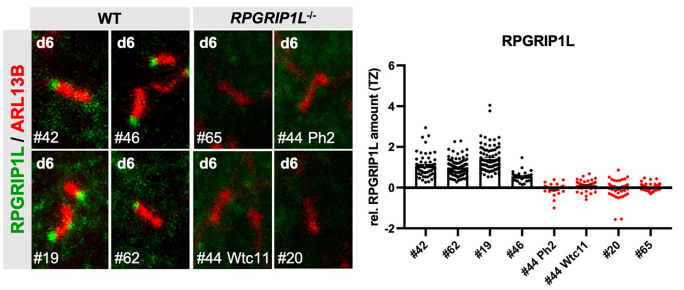

D

Name	CFD Score
ontarget_mm0_exon_**RPGRIP1L**_chr16_53730171_F	1.00
ontarget_mm0_exon_**RPGRIP1L**_chr16_53730171_R	1.00
mm4_exon_**NPRL2/CYB561D2**/XXcos-LUCA11.5_chr3_50385586_F	0.18
mm4_exon_**NPRL2/CYB561D2**/XXcos-LUCA11.5_chr3_50385586_R	0.18

E

```
           1                                                                                                                                                                                                                                                                                                                                                                                                                                                                                                                                                                                                                                                                                                                                                                                                                                                                                                                                                                                                                                                                                                                                                                                                                                                                                                                                                                                                                                                                                                                                                                                                                                                                                                                                                                                                                                                                                                                                                                                                                                                                                                                                                                                                                                                                                                                                                                                                                                                                                                                                                                                                                                                                                                                                                                                                                                                                                                                                                                                                                                                                                                                                                                                                                                                                                                                                                                                                                                                                                                                                                                                                                                                                                                                                                                                                                                                                                                                                                                                                                                                                                                                                                                                                                                                                                                                                                                                                                                                                                                                                                                                                                                                                                                                                                                                                                                                                                                                                                                                                                                                                                                                                                                                                                                                                                                                                                                                                                                                                                                                                                                                                                                                                                                                                                                                                                                                                                                                                                                                                                                                                                                                                                                                                                                                                                                                                                                                                                                                                                                                                                                                                                                                                                                                                                                                                                                                                                                                                                                                                                                                                                                                                                                                                                                                                                                                                                                                                                                                                                                                                                                                                                                                                                                                                                                                                                                                                                                                                                                                                                                                                                                                                                                                                                                                                                                                                                                                                                                                                                                                                                                                                                                                                                                                                                                                                                                                                                                                                
 RPGRIP1L                                                                                                                                                                                                                                                                                                                                                                                                                                                                                                                                                                                                                                                                                                                                                                                                                                                                                                                                                                                                                                                                                                                                                                                                                                                                                                                                                                                                                                                                                                                                                                                                                                                                                                                                                                                                                                                                                                                                                                                                                                                                                                                                                                                                                                                                                                                                                                                                                                                                                                                                                                                                                                                                                                                                                                                                                                                                                                                                                                                                                                                                                                                                                                                                                                                                                                                                                                                                                                                                                                                                                                                                                                                                                                                                                                                                                                                                                                                                                                                                                                                                                                                                                                                                                                                                                                                                                                                                                                                                                                                                                                                                                                                                                                                                                                                                                                                                                                                                                                                                                                                                                                                                                                                                                                                                                                                                                                                                                                                                                                                                                                                                                                                                                                                                                                                                                                                                                                                                                                                                                                                                                                                                                                                                                                                                                                                                                                                                                                                                                                                                                                                                                                                                                                                                                                                                                                                                                                                                                                                                                                                                                                                                                                                                                                                                                
 GRCh38.p14  CGTTCATCAACATGCTGCAGCTGCTGGGGGTGGCGGCCAATGAGGTCTCGCACGGTAGTGCCAGGGCTCAGGCTGCAGTATAGCTGGAACACATCCCGGAGACTGGCCCTCTTGTGCC
 Ph2_42      CGTTCATCAACATGCTGCAGCTGCTGGGGGTGGCGGCCAATGAGGTCTCGCACGGTAGTGCCAGGGCTCAGGCTGCAGTATAGCTGGAACACATCCCGGAGACTGGCCCTCTTGTGCC
 Ph2_46      CGTTCATCAACATGCTGCAGCTGCTGGGGGTGGCGGCCAATGAGGTCTCGCACGGTAGTGCCAGGGCTCAGGCTGCAGTATAGCTGGAACACATCCCGGAGACTGGCCCTCTTGTGCC
 Ph2_20      CGTTCATCAACATGCTGCAGCTGCTGGGGGTGGCGGCCAATGAGGTCTCGCACGGTAGTGCCAGGGCTCAGGCTGCAGTATAGCTGGAACACATCCCGGAGACTGGCCCTCTTGTGCC
 Ph2_44      CGTTCATCAACATGCTGCAGCTGCTGGGGGTGGCGGCCAATGAGGTCTCGCACGGTAGTGCCAGGGCTCAGGCTGCAGTATAGCTGGAACACATCCCGGAGACTGGCCCTCTTGTGCC
 Wtc11_19    CGTTCATCAACATGCTGCAGCTGCTGGGGGTGGCGGCCAATGAGGTCTCGCACGGTAGTGCCAGGGCTCAGGCTGCAGTATAGCTGGAACACATCCCGGAGACTGGCCCTCTTGTGCC
 Wtc11_62    CGTTCATCAACATGCTGCAGCTGCTGGGGGTGGCGGCCAATGAGGTCTCGCACGGTAGTGCCAGGGCTCAGGCTGCAGTATAGCTGGAACACATCCCGGAGACTGGCCCTCTTGTGCC
 Wtc11_44    CGTTCATCAACATGCTGCAGCTGCTGGGGGTGGCGGCCAATGAGGTCTCGCACGGTAGTGCCAGGGCTCAGGCTGCAGTATAGCTGGAACACATCCCGGAGACTGGCCCTCTTGTGCC
 Wtc11_65    CGTTCATCAACATGCTGCAGCTGCTGGGGGTGGCGGCCAATGAGGTCTCGCACGGTAGTGCCAGGGCTCAGGCTGCAGTATAGCTGGAACACATCCCGGAGACTGGCCCTCTTGTGCC
 Consensus   CGTTCATCAACATGCTGCAGCTGCTGGGGGTGGCGGCCAATGAGGTCTCGCACGGTAGTGCCAGGGCTCAGGCTGCAGTATAGCTGGAACACATCCCGGAGACTGGCCCTCTTGTGCC
```

Figure S3

A

Guide	Sequence + PAM	Crispr Score	Off Target
RPGRIP1L_exon3	ACGGACAATGAAGTCTCGCC AGG	92	0-0-0-8-38
RPGRIP1L_exon27	TATGCTTAGTTAGACGTGAA AGG	96	0-0-1-5-61

B

Cell line	Origin	# clone	Genotype	Method	Mutation
Ph2	PCli033-A	F6	+/-	KO	Δex3-ex27
Ph2	PCli033-A	C5	-/-	KO	Δex3-ex27 / Δex3-ex27

C

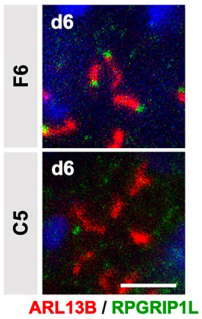

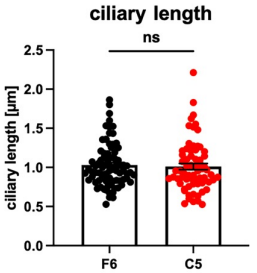

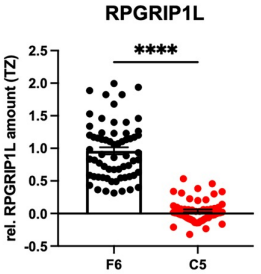

D

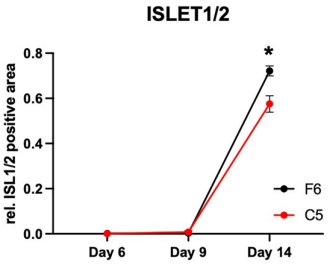

E

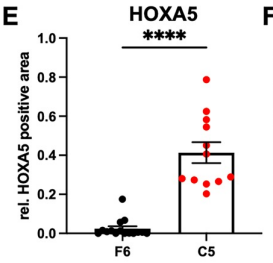

F

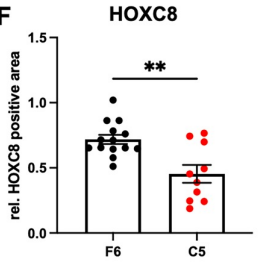

Figure S4

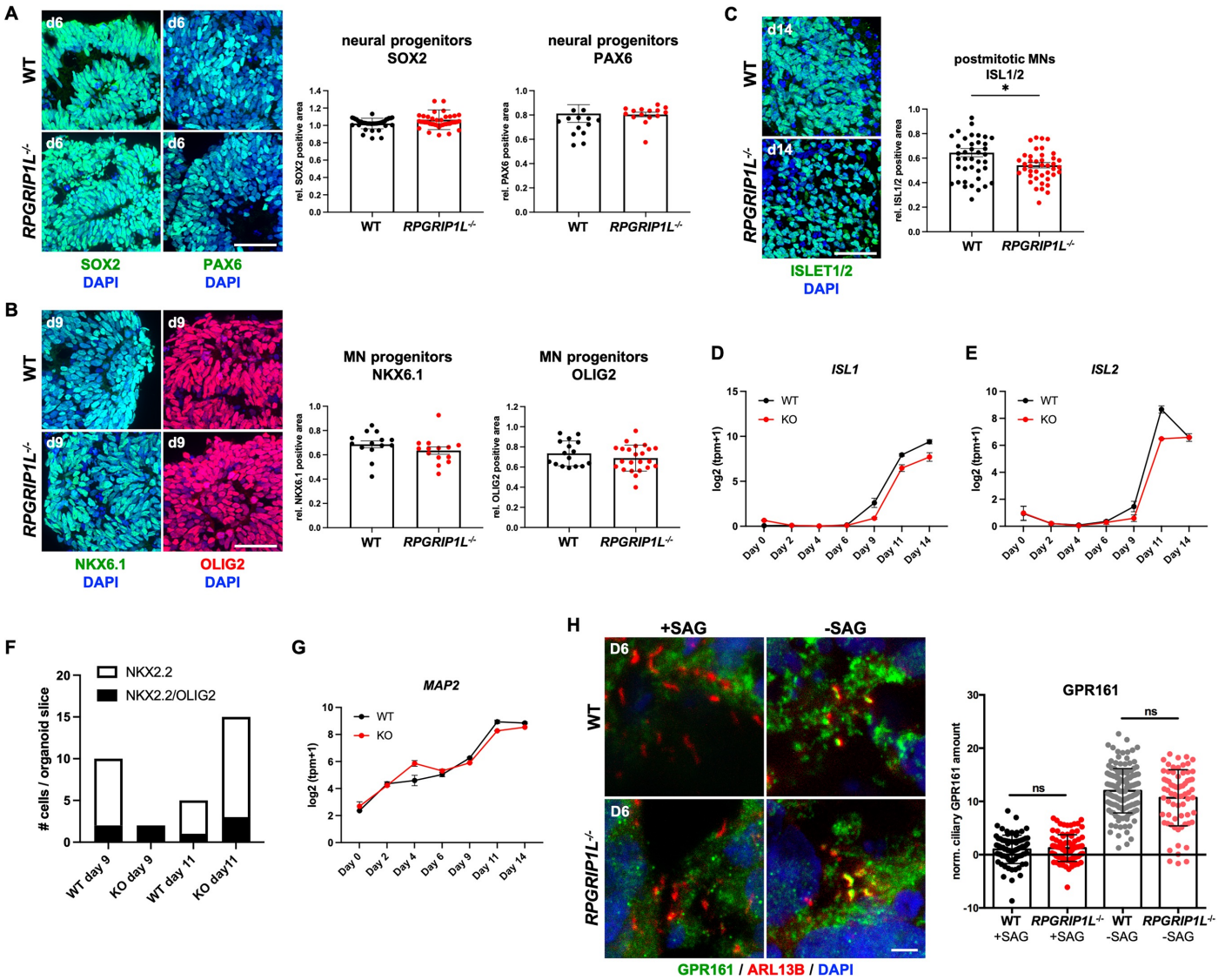
A
d6
WT
RPGRIP1L-/-
SOX2
DAPI
PAX6
DAPI
neural progenitors SOX2
rel. SOX2 positive area
neural progenitors PAX6
rel. PAX6 positive area
WT
RPGRIP1L-/-
B
d9
NKX6.1
DAPI
OLIG2
DAPI
MN progenitors NKX6.1
rel. NKX6.1 positive area
MN progenitors OLIG2
rel. OLIG2 positive area
C
d14
ISLET1/2
DAPI
postmitotic MNs ISL1/2
rel. ISL1/2 positive area
*
D
ISL1
log2 (tpm+1)
WT
KO
Day 0
Day 2
Day 4
Day 6
Day 9
Day 11
Day 14
E
ISL2
F
NKX2.2
NKX2.2/OLIG2
cells / organoid slice
WT day 9
KO day 9
WT day 11
KO day11
G
MAP2
H
+SAG
-SAG
D6
GPR161 / ARL13B / DAPI
GPR161
norm. ciliary GPR161 amount
ns
WT +SAG
RPGRIP1L-/- +SAG
WT -SAG
RPGRIP1L-/- -SAG

Figure S5

A

Guide	Sequence + PAM	Crispr Score	Off Target
TMEM67_exon1	GGTTAGAGACCGGTTAACCC TGG	97	0-0-0-1-21
TMEM67_exon27	ATCTCGGCGCTCACTAGCAG TGG	94	0-0-0-0-29

B

Cell line	Origin	# clone	Genotype	Method	Mutation
Ph2	PCli033-A	#1	+/-	KO	Δex1-ex27
Ph2	PCli033-A	#14	-/-	KO	Δex1-ex27 / Δex1-ex27

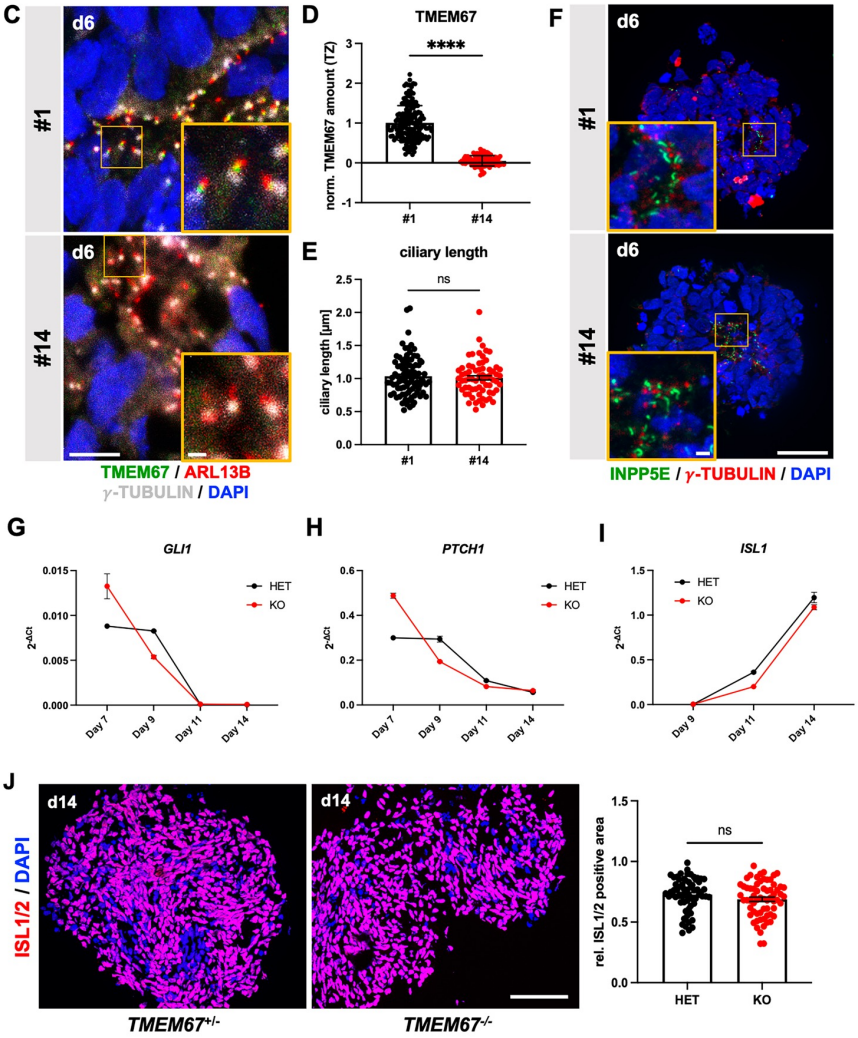

Figure S6

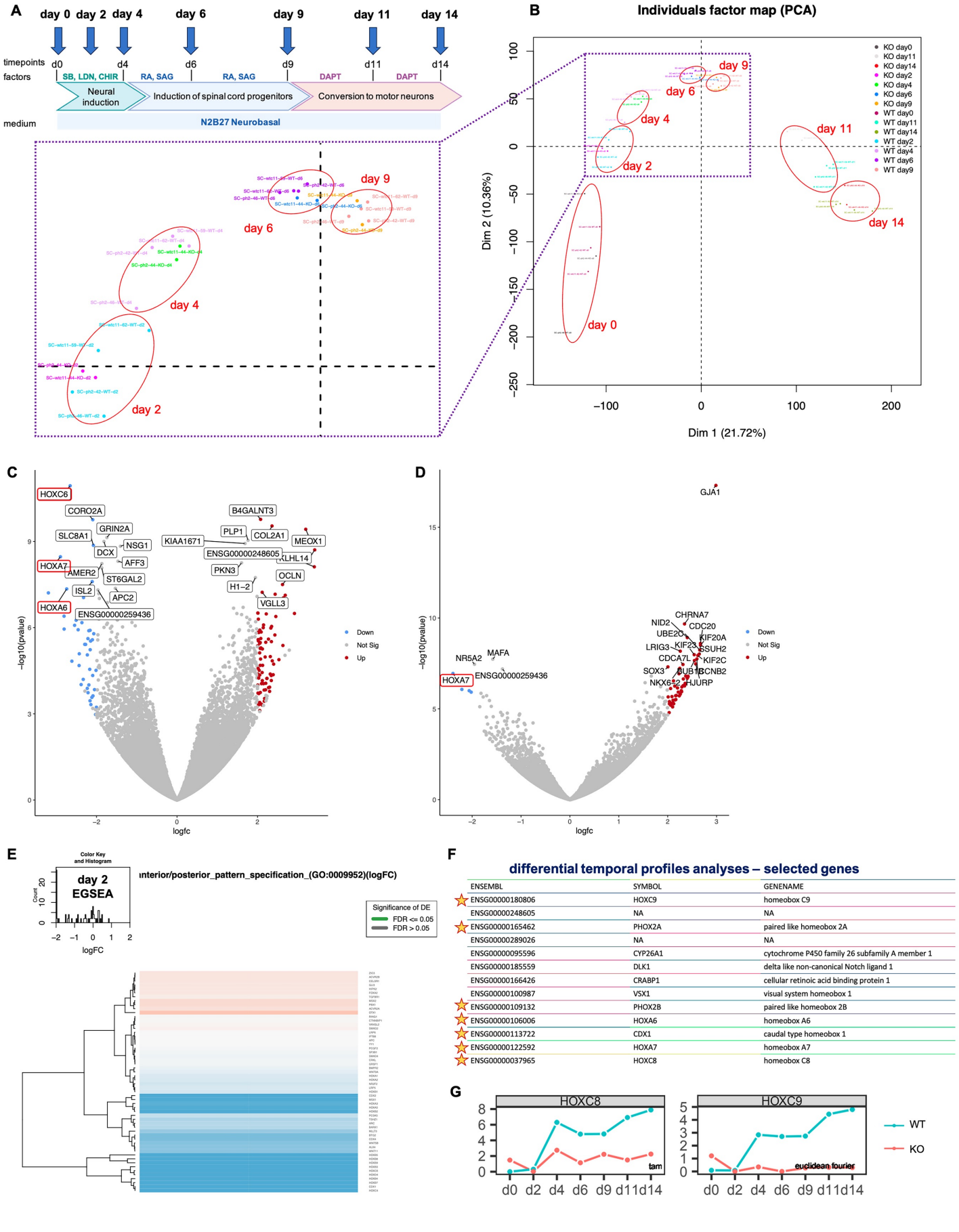

ENSEMBL	SYMBOL	GENENAME
ENSG00000180806	HOXC9	homeobox C9
ENSG00000248605	NA	NA
ENSG00000165462	PHOX2A	paired like homeobox 2A
ENSG00000289026	NA	NA
ENSG00000095596	CYP26A1	cytochrome P450 family 26 subfamily A member 1
ENSG00000185559	DLK1	delta like non-canonical Notch ligand 1
ENSG00000166426	CRABP1	cellular retinoic acid binding protein 1
ENSG00000100987	VSX1	visual system homeobox 1
ENSG00000109132	PHOX2B	paired like homeobox 2B
ENSG00000106006	HOXA6	homeobox A6
ENSG00000113722	CDX1	caudal type homeobox 1
ENSG00000122592	HOXA7	homeobox A7
ENSG00000037965	HOXC8	homeobox C8

Figure S7

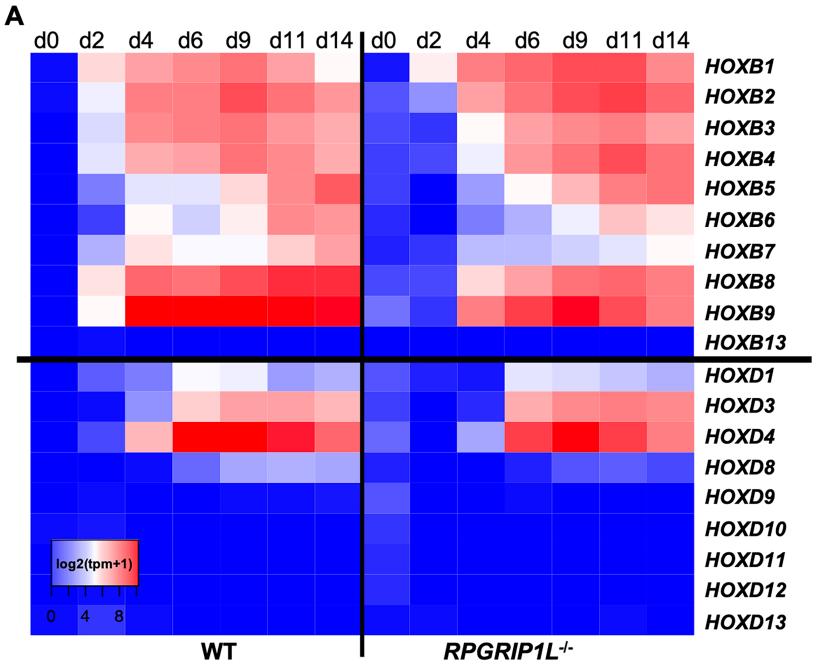
A
d0 d2 d4 d6 d9 d11 d14
d0 d2 d4 d6 d9 d11 d14
HOXB1
HOXB2
HOXB3
HOXB4
HOXB5
HOXB6
HOXB7
HOXB8
HOXB9
HOXB13
HOXD1
HOXD3
HOXD4
HOXD8
HOXD9
HOXD10
HOXD11
HOXD12
HOXD13
log2(tpm+1)
0 4 8
WT
RPGRIP1L-/-

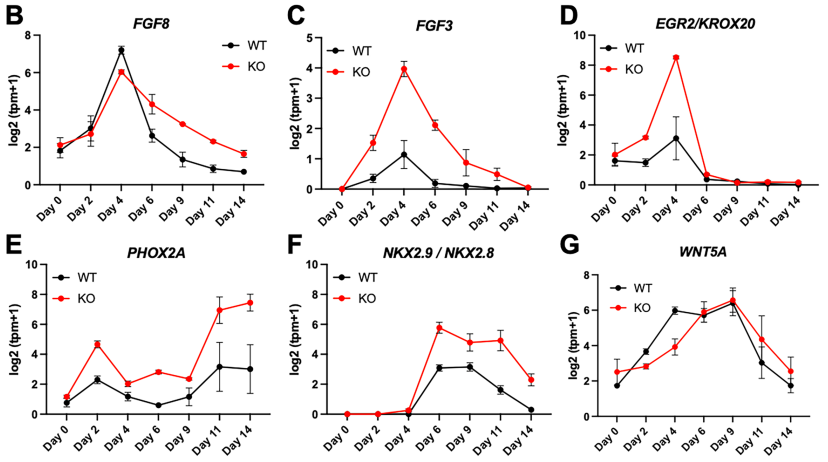
B
FGF8
C
FGF3
D
EGR2/KROX20
E
PHOX2A
F
NKX2.9 / NKX2.8
G
WNT5A
WT
KO
log2 (tpm+1)
Day 0
Day 2
Day 4
Day 6
Day 9
Day 11
Day 14

Figure S8

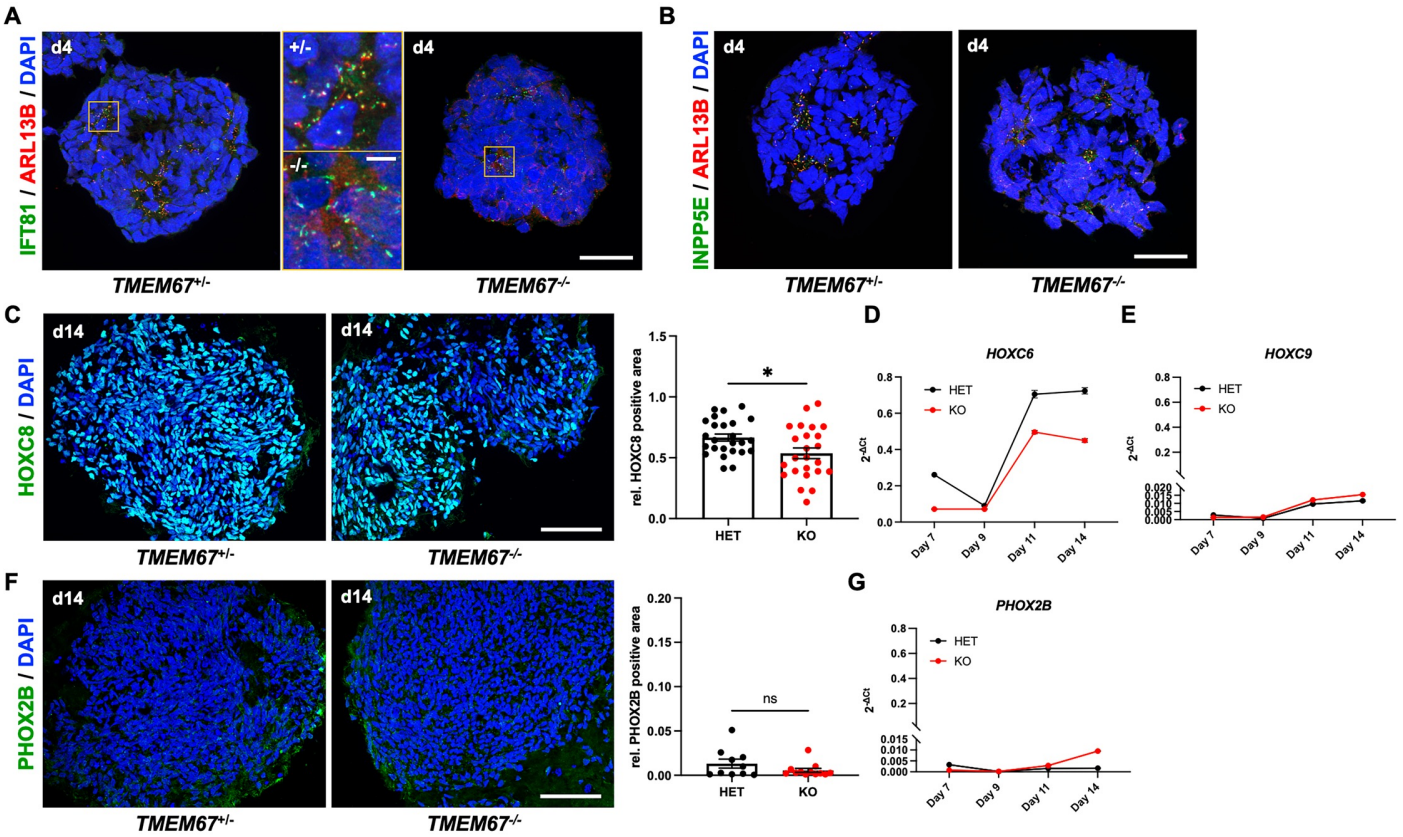
A
IFT81 / ARL13B / DAPI
d4
+/-
-/-
d4
TMEM67+/-
TMEM67-/-
B
INPP5E / ARL13B / DAPI
d4
d4
TMEM67+/-
TMEM67-/-
C
HOXC8 / DAPI
d14
d14
TMEM67+/-
TMEM67-/-
rel. HOXC8 positive area
1.5
1.0
0.5
0.0
*
HET
KO
D
HOXC6
HET
KO
2-ΔCt
0.8
0.6
0.4
0.2
0.0
Day 7
Day 9
Day 11
Day 14
E
HOXC9
HET
KO
2-ΔCt
0.8
0.6
0.4
0.2
0.020
0.015
0.010
0.005
0.000
Day 7
Day 9
Day 11
Day 14
F
PHOX2B / DAPI
d14
d14
TMEM67+/-
TMEM67-/-
rel. PHOX2B positive area
0.20
0.15
0.10
0.05
0.00
ns
HET
KO
G
PHOX2B
HET
KO
2-ΔCt
0.8
0.6
0.4
0.2
0.015
0.010
0.005
0.000
Day 7
Day 9
Day 11
Day 14

Figure S9

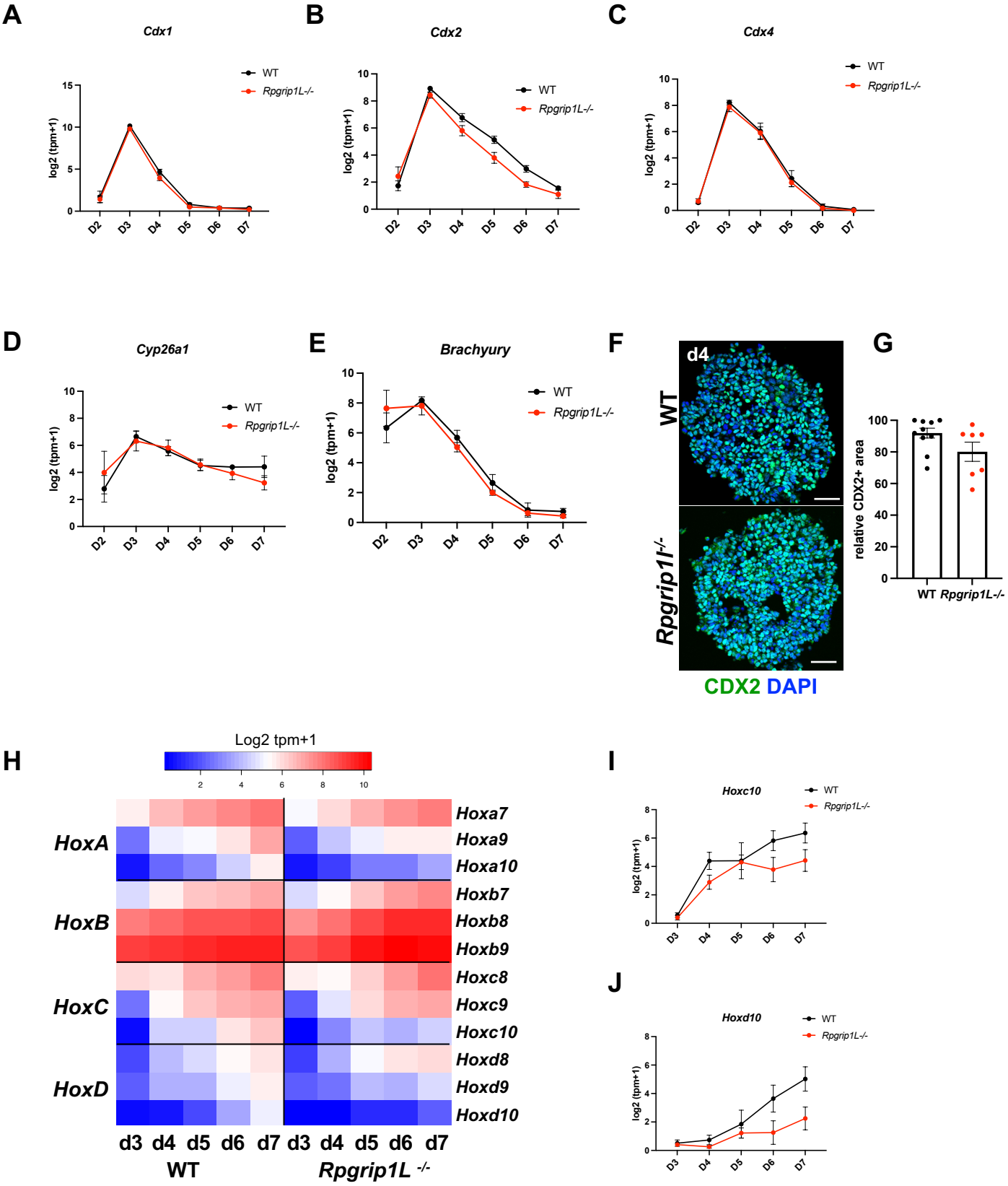
A
Cdx1
WT
Rpgrip1L-/-
log2 (tpm+1)
D2 D3 D4 D5 D6 D7
B
Cdx2
C
Cdx4
D
Cyp26a1
E
Brachyury
F
d4
WT
Rpgrip1l-/-
CDX2 DAPI
G
relative CDX2+ area
WT Rpgrip1L-/-
H
Log2 tpm+1
HoxA
HoxB
HoxC
HoxD
Hoxa7
Hoxa9
Hoxa10
Hoxb7
Hoxb8
Hoxb9
Hoxc8
Hoxc9
Hoxc10
Hoxd8
Hoxd9
Hoxd10
d3 d4 d5 d6 d7 d3 d4 d5 d6 d7
WT
Rpgrip1L -/-
I
Hoxc10
J
Hoxd10

qPCR			
Gene	**species**	**Forward**	**Reverse**
GLI1	human	CCCAGTACATGCTGGTGGTT	GCTTTACTGCAGCCCTCGT
PTCH1	human	GATGGGGCCATCTCCACATT	CGCCGCAAAGAAGTACCTTACA
OLIG2	human	GGGCCACAAGTTAGTTGGAA	GAGGAACGGCCACAGTTCTA
ISLET1	human	TGTTTGAAATGTGCGGAGTG	GCATTTGATCCCGTACAACC
NKX2.2	human	CTCCAGCTCGTAGGTCTGC	CAGGGTGCTCCGAGTCTG
HOXA5	human	GGAGATCATAGTTCCGTGAGC	GCTGAGATCCATGCATTGT
HOXC9	human	TCCTAGCGTCCAGGTTTCC	GCTACAGTCCGGCACCAA
PHOX2B	human	AACCCGATAAGGACCACTTTTG	AGAGTTTGTAAGGAACTGCGG
Sequencing			
Gene_region	**on/off-target**	**Forward**	**Reverse**
RPGRIP1L_exon3	on-target	TTTTATCCTCCTGCTTGCGG	AAGAACGGCACTTGAATACATTT
RPGRIP1L_exon27	on-target	TGTAATGGTGACCCAGGGATGT	AGAAGGAACATAGCCTGTTTGC
TMEM67_exon1	on-target	TGGGTTTTAAGTCAGTGGGGT	GTTGTTGTCGCACTTCTCCG
TMEM67_intron27	on-target	TGAAGTGGGACACAGTGGAAG	ATCCATGTTCATTGGCAGTGG
NPRL2_exon8	off-target	CAAGTCCCTGCAAGAGGCAT	CTCTGCTCTTCCCGAGTCAC

Table S1: qPCR and sequencing primer.

primary Antibody	host	company	reference		secondary Antibody	host	conjugate
Ac3	rabbit	Abcam	ab125093		Mouse IgG1	goat	Alexa488
Arl13b	mouse IgG2a	Antibody Incorporated	75-287		Mouse IgG1	goat	Alexa633
Brachyury	rabbit	Cell Signaling/Ozyme	81694		Mouse IgG2a	goat	Alexa488
Cdx2	rabbit	Abcam	ab76541		Mouse IgG2a	goat	Alexa594
Gpr161	rabbit	Proteintech	13398-1-AP		Mouse IgG2a	goat	Alexa633
Hoxa5	rabbit	Sigma	HPA029319		Mouse IgG2b	goat	Alexa488
Hoxc8	rabbit	Sigma	HPA028911		Mouse IgG2b	goat	Alexa594
Ift81	rabbit	Proteintech	11744-1-AP		Mouse IgG2b	goat	Alexa633
Ift88	rabbit	Proteintech	13967-1-AP		Rabbit	goat	Alexa488
Inpp5e	rabbit	Proteintech	17797-1-AP		Rabbit	goat	Alexa594
Islet1/2	mouse IgG2b	DSHB	39.4D5		Rabbit	goat	Alexa633
Nkx2.2	mouse IgG2b	DSHB	74.5A5				
Nkx6.1	mouse IgG1	DSHB	F55A12				
Olig2	rabbit	Millipore	AB9610				
Pax6	rabbit	BioLegend	PRB-278P				
Pax6	mouse IgG1	DSHB	PAX6				
FoxA2	mouse IgG1	DSHB	4C7				
Phox2b	rabbit	kindly provided by JF Brunet	/				
RPGRIP1L	rabbit	homemade anti-human	/				
Rpgrip1l	rabbit	homemade anti-mouse	/				
Sox2	rabbit	Millipore	AB5603				
Tmem67	rabbit	Proteintech	13975-1-AP				
Tuj1	mouse IgG2a	BioLegend	MMS-435P				
γ-Tubulin	mouse IgG1	Sigma	T6557				

Table S2: Primary and secondary Antibodies.